Modeling the influence of orbital forcing, greenhouse gases and Northern Hemisphere ice-sheets on Southern Hemisphere climate

Heike Gaasbeek
Student number: 0476374
h.gaasbeek@students.uu.nl
Westeinde 681, 2512 KK, Den Haag

Sustainable Development: Landuse, Environment and Biodiversity
45 ECTS

Universiteit Utrecht

Supervisors: Dr. Erik Tuenter and Dr. Stefan C. Dekker

Preface

I have done a course at Earth Sciences named astronomical forcings, and liked it so much that I have asked if there were any research topics that I could work on. I wanted to model and to work with astronomical cycles and in this way I came at the KNMI (Royal Netherlands Meteorological Institute) in De Bilt with Nanne Weber where I started the research. This research is the final assignment of the Master Sustainable Development: Land use, Environment and Biodiversity and I have been working on it for the last year. It has showed me again that I like doing research and I hope that in future I can keep on working in a research environment.

Of course this completing the research is done with the help of others that I would like to thank. First Erik Tuenter, my supervisor for the last period. I have learned very much about climate, climate response and orbital cycles, and also the absence of my "paleo jargon" was no problem for you. You always had the patience to explain and I am very grateful for all of your help with both the thesis and the presentation.

Secondly I would like to thank Nanne Weber, who was my supervisor when I just started the research. You helped me a lot with setting up the research and writing the research proposal.

Of course I also want to thank Stefan Dekker for reading the thesis in the finals stages and give feedback on the contents. It has helped to make it better.

Without the support from home it would have been possible to finish this research. First I want to thank my parents who have supported me with practical issues like the providing for a place to work, helping out with my sun and keeping me focused at the end. Secondly thanks for my brother Menco who I have promised to mention in the preface after babysitting on my sun, his nephew. Of course I would have mentioned you anyway, even without you babysitting.

Last but not least, Ishan my sun, my everything, that makes me go home with a smile and Sander, you have supported me throughout the research which was not in the most easiest period for me, but I am happy that you are here, and without you being there I could not have finished it!

Summary

To understand climate change an obvious first step is to understand the major climate shifts in history. All over the world in sediments deposited on land and on the bottom of the oceans, as well as from ice core measurements a regular pattern of glacial cycles is found. They are dominated by periods caused by variations in the orbit of the Earth and in the orientation of Earth's rotational axis, i.e., eccentricity (100,000 years (100 kyr)), obliquity (41 kyr) and precession (23 and 19 kyr).

Next to climate variations directly forced by orbital induced forced insolation changes, Earth's climate is also affected by variations in ice-sheets and greenhouse gas (GHG) concentrations. Both ice-sheet volumes as well as GHG-concentrations show large differences between glacials and interglacials. The timing of the mid-latitudinal glacials on the SH seems to be synchronous with the variations in NH ice-sheets. Still there is much debate about the relation between NH and SH climate on orbital timescales.

Here this issue is addressed by performing transient climate simulations for the last 650,000 years with a climate model of intermediate complexity (CLIMBER-2) that includes prescribed varying NH ice

sheets and greenhouse gas concentrations. Four different runs were performed to be able to study the influence of orbital forcing alone (with fixed NH ice sheets and GHG-concentrations) as well as the combined influence of orbital forcing and NH ice-sheets and/or GHG-concentrations. The studied SH climate variables are low-latitudinal monsoonal precipitation averaged over December-January-February (DJF), annual Surface Air Temperature (SAT) at low, mid- and high latitudes, annual Sea Surface Temperature (SST) at low and mid-latitudes and annual sea-ice.

The results show that if climate is only forced by orbital induced insolation changes the variability is only determined by obliquity and precession with dominance of obliquity at high latitudes and precession at low latitudes. Adding GHG-concentrations and/or NH-ice sheets generally results in a dominant 95 kyr component for the annual SAT, SST and sea-ice at all latitudes. The exception is the seasonal monsoonal precipitation that is still dominated by precession and SAT at high latitudes that is still dominated by obliquity if only NH ice-sheets are introduced (i.e., GHG-concentrations are fixed). At low latitudes temperatures are equally affected by varying GHG-concentrations and NH ice-sheets while at high latitudes GHG-concentrations is the dominant forcing.

At the precession band the monsoonal precipitation leads precession by about 700 years with orbital forcing only which is barely influenced by GHG and NH ice sheets. The lag of the annual SAT and SST at mid- and high latitude of about 1 kyr with orbital forcing only increases to about 3-4 kyr if GHG-concentrations and NH ice-sheets are introduced. At the obliquity band the phase difference vary from very small with orbital forcing only to about 4-5 kyr including NH ice sheets and GHG-concentrations.

Comparison of Antarctic Deuterium measurements to the simulated Antarctic SAT from the model results showed that orbital forcing alone cannot explain the Antarctic temperature and that both NH ice-sheets and greenhouse gas concentrations are necessary with a larger influence of the GHG-concentrations compared to NH ice-sheets. In the fully forced simulation CLIMBER-2 is able to accurately simulate the (unfiltered) Antarctic temperature derived from Deuterium (correlation 0.87) which improves significantly if only obliquity and the 95 kyr components are taken into account (correlation ~0.97).

Samenvatting

Om klimaatverandering te begrijpen is het eerst belangrijk om grote klimaatverschuivingen uit de geschiedenis te kunnen begrijpen. In sedimenten die gevonden zijn op land en in oceanen, evenals in ijskernen, zijn regelmatige patronen gevonden van glacialen. Al in de jaren ’70 van de vorige eeuw hebben wetenschappers bewijzen gevonden dat variaties in de baan van de aarde de belangrijkste oorzaak zijn van deze cycli. Deze glacialen worden geforceerd door veranderingen in de stand van de aarde ten opzichte van de zon, d.w.z. de eccentriciteit (met een periode van 100,000 jaar), de obliquiteit (41,000 jaar) en precessie (23,000 jaar). Deze periodes zijn zowel op de noordelijke als op het zuidelijke halfrond gevonden.

Naast deze klimaatveranderingen veroorzaakt door orbitaal veranderingen, wordt het klimaat ook beïnvloed door variaties in broeikasgassen en ijsvolumes. De timing van deze glacialen op het noordelijk halfrond ligt gelijk met die van het zuidelijk halfrond. Dit geeft nog steeds veel onzekerheid over de relaties tussen het noordelijk halfrond en zuidelijk halfrond.

In dit onderzoek is dit onderwerp onderzocht door middel van de analyse van zeer lange klimaatsimulaties uitgevoerd met een klimaatmodel Climber. Er zijn vier verschillende scenario's, één met variërend orbitaal signaal, en de broeikasgassen (280 ppmv) en ijskappen (op huidige niveaus) constant. In het tweede scenario variëren en het orbitaal signaal en de ijskappen, maar de broeikasgassen blijven constant. In het derde scenario variëren het orbitaal signaal en de broeikasgassen en blijven de ijskappen constant en in het laatste scenario, variëren ze alle drie.
De bestudeerde klimaatvariabelen zijn; de moesson gebieden op het zuidelijk halfrond (15°S) gemiddeld over December-Januari-Februari, de jaarlijkse luchttemperatuur aan de oppervlakte (lage midden en hoge breedtes), de jaarlijkse zeetemperatuur (lage en midden breedtes) en het jaarlijkse zee-ijs.
De resultaten laten zien dat wanneer alleen geforceerd door orbitaal veranderingen, het klimaat beïnvloed wordt door precessie en obliquiteit, met obliquiteit als dominante factor op hoge breedtes en precessie dominant op de lagere breedtes. Wanneer broeikasgassen en/of ijskappen worden toegevoegd, worden zeetemperatuur, oppervlakte temperatuur en zee-ijs gedomineerd door een 95,000 jaar component. Op lage breedtes worden temperaturen evenveel door broeikasgassen als ijskappen bepaald, terwijl op hogere breedtes de broeikasgassen de bepalende factor worden. De seizoensgebonden moessons zijn een uitzondering op de regel, Deze blijven gedomineerd door precessie hoewel er wel een 95,000 signaal bij komt door het toevoegen van broeikasgassen en ijskappen. Ook de oppervlakte temperaturen op hoge breedtegraden blijven door obliquiteit gedomineerd wanneer het model alleen door alleen ijskappen en orbitaal veranderingen wordt geforceeerd (broeikasgassen blijven constant).
De moessons op het zuidelijk halfrond lopen vooruit op het precessie signaal en dit verandert minimaal wanneer ook broeikasgassen en/of ijskappen worden toegevoegd. De vertraagde reactie van de temperatuur (zee en oppervlakte) van ongeveer 1000 jaar op precessie wordt groter wanneer ijskappen en/of broeikasgassen worden toegevoegd tot maximaal 4000 jaar. De faseverschillen op obliquiteit, variëren van 1000 jaar wanneer alleen geforceerd door orbitaal veranderingen tot 4000-5000 jaar met de invloed van broeikasgassen en ijskappen.
Vergelijkingen van modelresultaten met Deuterium metingen uit ijskernen van Antarctica laten zien dat klimaat alleen geforceerd door orbitaal variaties niet overeenkomt met de temperaturen gevonden op Antarctica. Broeikasgassen en ijskappen zijn beide nodig om de temperaturen te verklaren. Wanneer het model is geforceerd door orbitaal, broeikasgassen en ijskap variaties, worden temperaturen op Antarctica zoals gevonden in de Deuterium (correlatie 0,87) goed gesimuleerd. Wanneer dit signaal gefilterd wordt op obliquiteit en 95,000 worden de correlaties veel beter (~0,97).

Contents

1. Introduction

Today Earth's climate is rapidly warming and there is much debate if humans are the major cause of this. There is a lot of research to the extent of this warming. Studies show that the climate change observed in the recent past is not as drastic as the changes over longer periods (of ten to hundred thousands of years and more) (Ruddiman, 2008).

To understand climate change an obvious first step is to understand the major climate shifts in history. In sediment deposited on land and on the bottom of the oceans as well as from ice cores a regular patterns of glacial and interglacial cycles were found (Ruddiman, 2008; Weirt, 2008). A lot of effort has been made to study and explain these glacial cycles. Already in the late 70's of the last century scientists found evidence that variations in the orbit of the Earth are the major cause for the glacial cycles. They investigated $d^{18}O$ records in deep see sediments reflecting global ice volumes and deep-sea temperatures during the last million years. In these climatic records they identified a 41 kyr (41.000 years) climate component with the same period as obliquity, a 23 kyr component that displays the same periods (about 23 kyr and 19 kyr) as the quasi periodic precessions index and a 100 kyr component with an average period similar to eccentricity. These periods are found in climate records on the Northern Hemisphere (NH) as well as on the Southern Hemisphere (SH) (Hays et al. 1976; Imbrie and Imbrie, 1979).

Milankovitch (1941) was the first to suggest that orbital induced variations in summer insolation could control the volumes of the ice sheets. No matter how much snow falls or ice grows, it easily melts away when the following summer is warm. Therefore colder summers with low insolation cause the snow and ice to persist from one winter to the next. This is referred to as the Milankovitch theory of summer insolation (Ruddiman 2008). The latitude most sensitive to these insolation changes is 65^0N. At this latitude the amount of summer insolation can vary by as much as ± 12% around a long term mean value. Research shows that it is the area where the snow first accumulates and last melts (Hayes et al. 1976; Ruddiman, 2008).

Orbital Parameters

The orbital parameters are shown in Figure 1.

Obliquity

The obliquity, i.e. tilt, can be defined by the angle (in degrees) between the rotational axis of the Earth and a line perpendicular to the plane of the elliptic (Figure 1). The tilt together with the yearly circular motion of the Earth around the Sun causes the occurrence of seasons. Because the Earth is not a perfect sphere, the moon and the Suns gravities pull on the equatorial bulge and cause a change in the tilt. Today this tilt is about 23.5° but it has changed over the last million years between 22° and 24.5°. The dominant period of obliquity is 41 kyr (Ruddiman, 2008; Tuenter, 2004).

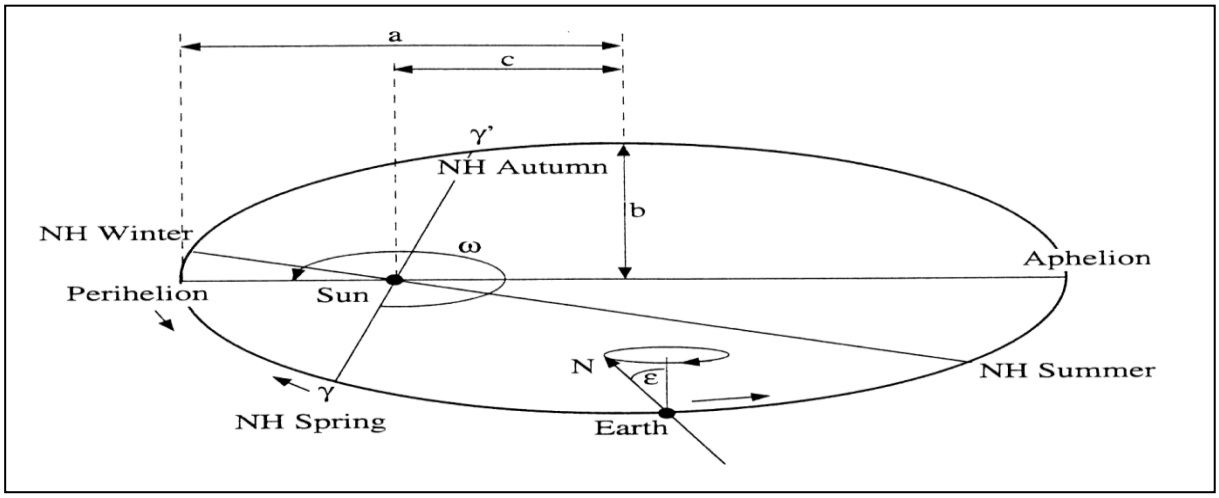

Figure 1: The orbital parameters of the Earth. a is the semi-major axis and b the semi-minor axis. Winter and summer solstice occurs respectively at the locations NH Winter and NH Summer. γ *is the vernal and* γ' *is the autumnal equinox while* ε *is the obliquity. Today the Earth is at perihelion (position of the Earth closest to the Sun) around the 3th of January. This position is measured by ω, the angle between the vernal equinox and perihelion (from Paillard, 2001, p 328).*

Eccentricity

The orbit of the Earth around the Sun is an ellipse (Figure 1). The Sun is located in one of the two focal points. Eccentricity of the Earth's orbit is described in equation 1 as:

$$e = \frac{\sqrt{a^2 - b^2}}{a} \qquad (1)$$

where *e* (no dimension) is the eccentricity and a (km) and b (km) the half lengths of the major and minor axes, i.e. semimajor and semiminor axes, respectively. When the difference in length between the two axes increases, the eccentricity increases while eccentricity drops to near zero if the length of the axes are almost equal (i.e. then the orbit of the Earth is near circular) (Ruddiman, 2008). The dominant component in the eccentricity is 413 kyr and the next four periods range from 95 kyr till 131 kyr which contribute to a peak, often referred as the 100 kyr eccentricity cycle (Tuenter, 2004). There is a sixth period of 2.3 Myr (million years) which has been observed in very long geological records (Tuenter, 2004).

Precession

The equinoxes are the locations of the Earth at its orbit when the days are as long as the nights (at all latitudes). It occurs around 21 March, i.e. vernal equinox, and around 21 September (autumnal equinox). The summer or winter solstices are defined as the position of the Earth perpendicular to respectively the tropics of Capricorn (23.45°N) around 21 June or the tropics of Cancer (23.45°S) around 21 December (Tuenter, 2004).

The movement of the Earth can be best compared with the motion of a spinning top (Figure 1). This motion exists of two separate movements, i.e., a fast spinning motion around its own axis and a slow wobbling motion gradually leaning in different directions through time. The wobbling motion of the Earth is called the axial precession which is caused by the gravity of the Sun and the moon and has a period of 25.7 kyr. This movement causes the equinoxes (and solstices) to move in a clockwise movement along the Earth's orbit and is therefore also called precession of the equinoxes. At the

same time the elliptical Earth orbit moves counterclockwise. This is called precession of the ellipse, and has a period of 75 kyr (Tuenter, 2004; Ruddiman, 2008).
The combined effect of the precession of the equinoxes and of the ellipse causes a counterclockwise movement of the solstices and equinoxes which is referred to as climatic precession. Only the combined movement affects the insolation received by the Earth. The periods of this movement consist of a strong 23 kyr component and a weaker 19 kyr component resulting in a period of climatic precession of about 21 kyr (Tuenter, 2004; Ruddiman 2008).
Eccentricity plays a large role in the effect of precession therefore its usual to combine them. When the eccentricity is zero, perihelion is not defined and there is no effect on the insolation with changing precession. The precession parameter is defined in equation 2 as:

$$Precession\ parameter = e\ sin(\pi + \omega) \qquad (2)$$

where ω is the angle between the vernal equinox and perihelion (in degrees) and e the eccentricity. The precession parameter (no dimension) is at its minimum when ω = 90°, i.e. when summer solstice occurs at perihelion and $e\ sin(\pi + \omega)$ is negative. Maximum precession occurs when winter solstice occurs at perihelion and ω = 270° with $e\ sin(\pi + \omega)$ positive (Tuenter, 2004).

The long term evolution of obliquity, eccentricity and precession makes it possible to calculate the amount of insolation arriving at any latitude and season. The June and December monthly insolation curves show a strong dominant 23 kyr precession signal at lower and middle latitudes and only in the summer season at high latitudes. The obliquity signal is not evident at the lower latitudes but clearly visible in at higher latitudes (Tuenter, 2004). To illustrate the influence of precession and obliquity on insolation at all latitudes, Tuenter (2004) showed the zonally averaged insolation difference between two extremes (minimum precession minus maximum precession and maximum obliquity minus minimum obliquity) (Figure 2). In the NH summer the insolation is much higher during minimum precession (positive in Figure 2a) because the NH summer is located at perihelion, while during maximum precession the NH summer is at aphelion. In the NH winter this effect is reversed leading to enhanced seasonal contrast, i.e. warmer summers and colder winters during minimum precession while at the same time the seasonality is reduced on the SH. For obliquity the figure shows enhanced seasonal contrast from low to high obliquity on both hemispheres (positive in Figure 2b) (Tuenter 2004).
Next to climate variations directly induced by orbital forced insolation changes, Earth's climate is also affected by variations in ice-sheets and greenhouse gas (GHG) concentrations. Both ice-sheet volumes as well as GHG-concentrations show large differences between glacial and interglacial's (Peltier, 2004; Lüthi et al., 2008; Loulergue et al., 2008). Possible non-linear effects of the climate responses to different forcings cause a very complex behavior of the climate system on orbital time-scales. A complicating factor is the occurrence of phase differences between the forcings and the response of the climate which has been found in proxy records (Yin et al., 2009; Ziegler et al., 2010; Clemens et al., 2010).
Climate records show connections between the NH and the SH, probably determined by climate responses to the orbital forcings (Crucifix et al, 2006). Analysis of phase relations by means of modeling and between different paleoclimatic records are still the most used methods to propose and test hypotheses about mechanisms of past climate change. Patterns and phases of climate responses provide a way to extract key cause and effect relationships in the climate system

(Ruddiman, 2003; Tuenter, 2004; Ruddiman, 2006; Ganopolski and Roche, 2009). Due to the high computationally costs climate model studies dealing with leads/lags on orbital timescales are not very numerous (e.g., Tuenter 2004; Kutzbach et al., 2008; Ganopolski and Roche, 2009; Weber and Tuenter, 2011). Some studies also examined orbital phase differences using statistical methods (Mudelsee, 2001; Hargreaves and Abe-Ouchi, 2003).

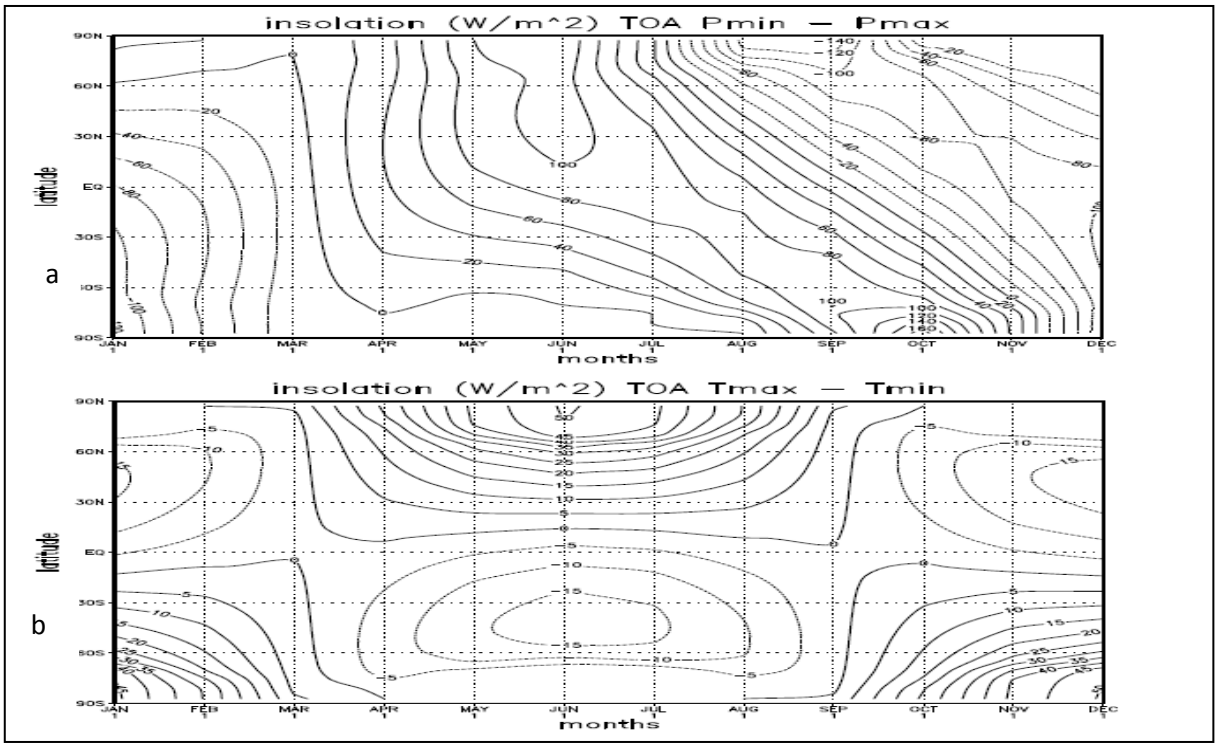

Figure 2 (a) Insolation differences when precession is at minimum minus the insolation when precession is at maximum. Obliquity is fixed to isolate the precession influence; (b) Insolation when obliquity is at maximum minus insolation when obliquity is at a minimum. To exclude the effect of precession, eccentricity is set at zero, i.e. a circular motion around the sun (from Tuenter 2004, p11).

Nelson et al. (1985) analyzed the relation between a glacier in New Zealand and the NH ice-sheets and found that the timing of the mid-latitudinal glacials on the SH appears to be synchronous with the changing NH ice-sheets. This requires a rapid transfer from the cooling of the NH into the SH. These results are unexpected because when SH climate is only forced by insolation changes as for the NH, as proposed by Milankovitch, the response of the SH climate should be out of phase with the NH response (Berger et al., 1993)

A modeling study of Broccoli and Manabe (1987) suggests that both CO_2 and NH ice-sheets are required to produce sufficient cooling on global basis, while the expansion of the NH ice-sheets alone has no substantial influence on the SH temperatures. Most cooling on the SH was caused by the reduction of CO_2, but this reduction could be triggered by the NH glaciations.

Imbrie et al. (1989) also showed that only the Northern summer insolation satisfies the ice sheet response at both the precession and the obliquity periods. They suggest that summer radiation forces the climate at the NH and that the signal is transferred to the higher latitudes at the SH.

Waelbroeck et al. (1995) found clear leads in the Antarctic air temperature compared to global ice volume in the obliquity and precession bands. Secondly, phase analysis between the filtered δD

(deuterium) and insolation at the precession band indicates a relation between the SH high latitude surface air temperatures and the changes in boreal summer insolation taking at NH low latitudes.
These studies discussed a relation between the NH glacials (forced by the summer insolation as proposed by Milankovitch) and GHG-concentrations with SH climate. Still there is much debate about relation between the NH climate and the SH climate. This research will focus on the relation between the NH and SH with the focus on the orbital forcings, NH ice-sheets and GHG-concentrations.

The research question for this study is:

What are the influences of orbital cycles, varying greenhouse gas-concentrations and Northern Hemisphere ice-sheets on the Southern Hemisphere climate?

The sub-questions are:
Where on the SH is the influence of varying ice sheets and/or varying GHG-concentrations$_2$ strongest and what is the influence of obliquity and precession at these locations?
What are differences in the climate response to only orbital induced insolation changes and to orbital induced insolation changes together with varying GHG-concentration and/or varying NH ice-sheets?
What are the main periods found in the different scenarios, and what are the similarities/differences between them?
What are the leads/lags of the climate response compared to the orbital forcing and/or the other forcings, i.e. varying GHG-concentrations and NH ice-sheets?

In chapter two the methods are explained, with first a short description of the model and the forcings that are used followed by an explanation of the analyses. In chapter three the results are presented followed by the discussion (chapter four) and the conclusion (chapter five) where the research question will be answered.

2. Methods

2.1 Model and the experimental set-up

At the KNMI (Royal Netherlands Meteorological Institute) in De Bilt (the Netherlands) transient climate model simulations have been performed with a model of intermediate complexity (CLIMBER-2) over the period of the last 650,000 years. The climate model consists of a statistical dynamical atmospheric component and a 3-basin zonally averaged ocean component including sea ice and a terrestrial dynamic vegetation model. It does not contain a dynamic ice sheet component and no carbon cycle model. The atmosphere has a resolution of 10° in latitude and 51° in longitude as shown in Figure 3. A detailed description of the model can be found in Petoukhov et al. (2000). The model has been successful in simulating cold climates as well as orbital-forced warmer periods like the mid-Holocene and results compare well with the observations of the modern climate (Ganopolski et al. 1998a; Ganopolski et al. 1998b; Petoukhov et al, 2000).

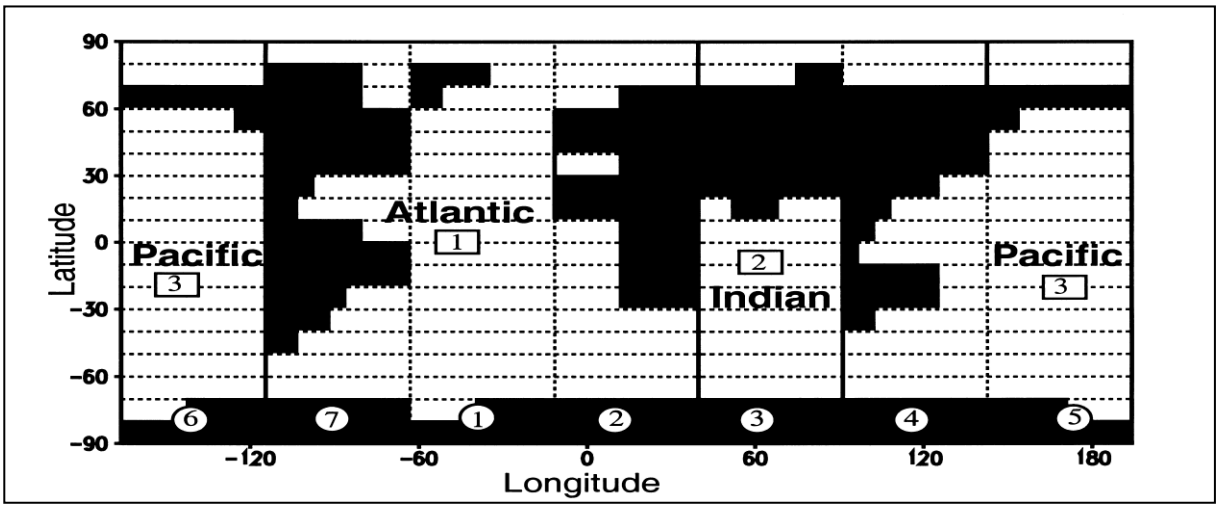

Figure 3: The representation of the Earth in CLIMBER-2. The horizontal and vertical lines represent the separate grid cells for the atmospheric part (10° in latitude and 51° in longitude). The atmospheric sectors are numbered in the circles. The solid vertical lines separate the three ocean basins which are numbered in the squares. The latitudinal resolution for the ocean is 2.5° (from Tuenter 2004, p47).

Four transient simulations are performed (Table 1). In all simulations orbital forcing, i.e., precession, obliquity and eccentricity as computed following Laskar et al. (2004) is used as forcing (Figure 4a). In run O the orbital forcing is the only forcing while GHG-concentrations are fixed at pre-industrial values (280 ppmv (parts per million volume) and the NH ice-sheets at present-day levels. In run OI varying NH ice-sheets (Bintanja et al., 2005) (Figure 4b) with fixed GHG-concentrations were used. In run OG the ice sheets are kept fixed with varying GHG-concentrations (Robertson et al., 2001; Lüthi et al.; 2008; Loulergue et al., 2008) (Figure 4b). Finally, in run OIG ice sheets, greenhouse gas concentrations and orbital forcings vary.

NH Ice sheet variations (both height and area) are prescribed based on earlier modeling work with a 3-dimensional ice sheet model coupled to a model of deep ocean temperature (Bintanja et al., 2005). Only the Laurentide and Eurasian ice sheet vary in time. The Antarctic and Greenland ice sheet are kept fixed at present-day values in all four runs. For the variations in greenhouse gases (a combination of CO_2 and CH_4) the EPICA ice core from Antarctica is used as source together with other sources for the more recent years (Robertson et al., 2001; Lüthi et al., 2008; Loulergue et al., 2008). In the used version, no carbon cycle is included meaning that different levels of CO_2 only influence the greenhouse gas effect and do not affect vegetation growth directly.

The results will be shown as averages over 100 years as the period of the forcings are much larger than 100 years. See Weber and Tuenter, 2011 for an extensive description of the experimental set-up.

Experiment	Orbital forcing	GHG-concentrations	Ice-sheet volumes
Run O	Variable (fig 4a)	Fixed (280 ppmv)	Fixed (present-day)
Run OG	Variable (fig 4a)	Variable (fig 4b)	Fixed (present-day)
Run OI	Variable (fig 4a)	Fixed (280 ppmv)	Variable (fig 4b)
Run OIG	Variable (fig 4a)	Variable (fig 4b)	Variable (fig 4b)

Table 1: Summary of the forcings as used in the four runs.

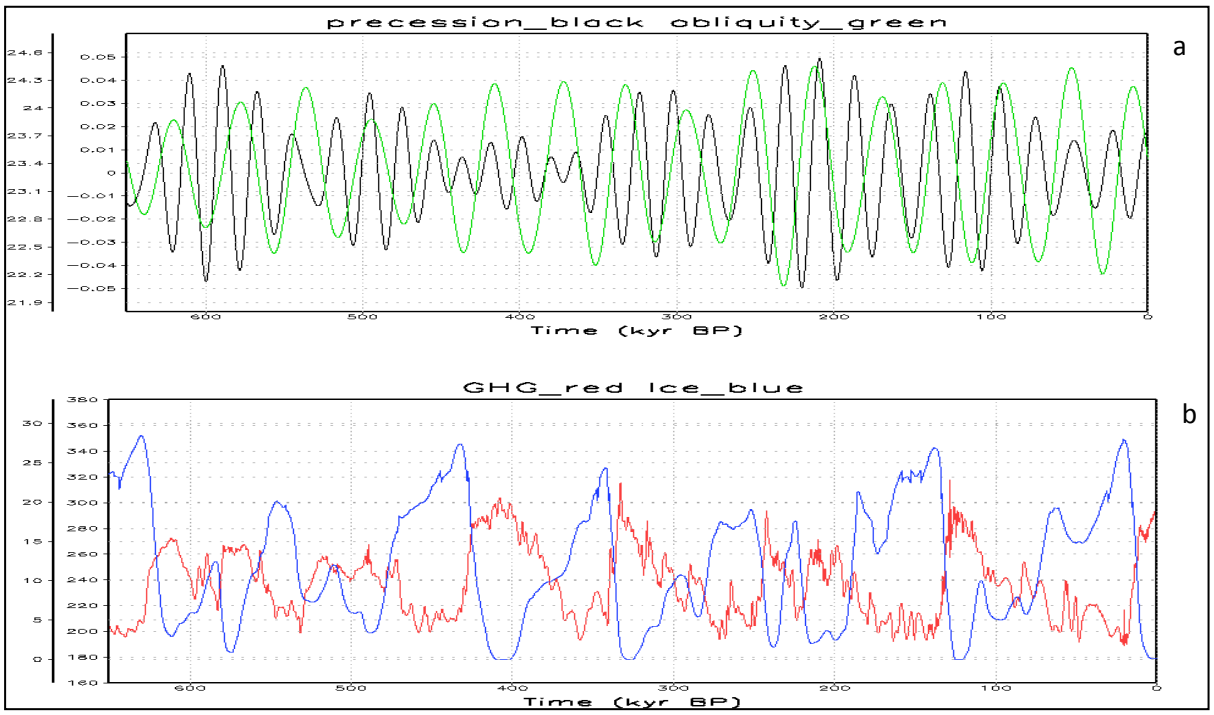

Figure 4: (a): Timeseries of the orbital forcings, precession in black (most right vertical axis) and obliquity (in degrees) in green (most left vertical axis); (b): Sum of the NH ice-sheet volumes (Laurentide and Eurasian, in million cubic kilometers) in blue (most left vertical axis) and the GHG-concentrations (in ppmv) in red most (right vertical axis) over the last 650.000 years (horizontal axis).

2.2 Data analysis

The data is analyzed with the visualization program GraDs. See appendix I for the output parameters of CLIMBER-2. Because there is such a large output dataset, a selection is made. As will be shown in the results section, Sea Surface Temperature (SST), precipitation, Surface Air Temperature (SAT) at 2 meters height and sea ice are analyzed because they react strongest to orbital forcing, NH ice-sheets and GHG-concentrations.

In order to investigate the effect of the orbital forcing on the SH climate the extreme maximum and minimum values of the obliquity and precession are taken A similar approach has been done for the effects of ice-sheet volumes and greenhouse gas concentrations, i.e. a time step with maximum ice sheet volume (GHG-concentration) compared to a time step with minimum ice-sheet volume (GHG-concentration). See Table 2 for the time of occurrence for the maxima and minima.

Forcing	Maximum	Minimum
Obliquity	213 kyr BP	232 kyr BP
Precession	210.5 kyr BP	220 kyr BP
GHG-concentrations	406 kyr BP	358 kyr BP
NH-ice sheets	432.5 kyr BP	405 kyr BP

Table 2: Parameters used for the global results, showing the occurrence (in kyr before present) of extreme values of obliquity, precession, GHG-concentrations and NH ice sheets.

After identifying the most interesting areas on the SH from the global results, timeseries for 650 kyr until present for these areas are made. To determine the dominant periods, Blackman-Tukey spectral analyses were performed using Analyseries software (Paillard et al., 1996).
To extract these dominant periods from the timeseries, the periods were filtered using Analyseries (Paillard et al., 1996), see Table 3 for the applied periods, frequencies and bandwidths. Cross-correlation between these filtered climate variables and the filtered forcings reveals the accuracy of the relations (determined by the height of the correlations) as well as the phase differences between the forcings and the climate response

	Precession	**obliquity**	**95 kyr**
Period (kyr)	23,3	41.7	95.2
Frequency (1/kyr)	0.043	0.024	0.0105
Bandwidth (1/kyr)	0.0037	0.0012	0.00021

Table 3: Periods, frequencies and bandwidths as used for the filtering.

To study the accuracy of the simulated climate, a comparison is made between the results of SAT at high SH latitudes and a Deuterium record. Deuterium shows a strong spatial correlation between annual mean temperature and the mean isotopic fraction of the ^{2}H in precipitation (Stenni et al., 2003). This makes it possible to use Deuterium as proxy for surface air temperature. Earlier research has showed linear relationships between annual surface temperatures and snow deuterium content (Stenni et al., 2003; Jouzel, 2004).

A Deuterium record from dome Epica C (European Project for Ice Coring in Antarctica) at $75^{0}S;123^{0}E$ is used (Jouzel et al., 2007) which extends to 800,000 years BP. The record is converted using cubic spline interpolations to 6500 timesteps identifying the last 650 kyr in the same way Climber does. The spectral analyses, timeseries and filtered timeseries of the deuterium record are compared to corresponding annual SAT at $85^{0}S$ from all runs.

3. Results

3.1 Spatial results

Figure 5 shows the modeled results for present-day from, run OIG. The model simulates the SH summer monsoons (African, Australian and South-American) and the weak precipitation at high SH latitudes. The latitudinal border for sea-ice is 60°S with the smallest amount over the Atlantic Ocean and the largest amount over the Pacific Ocean. Both SAT and SST show a strong meridional gradient with very low SAT over Antarctica while the SST is around -1°C over the sea-ice covered SH ocean.

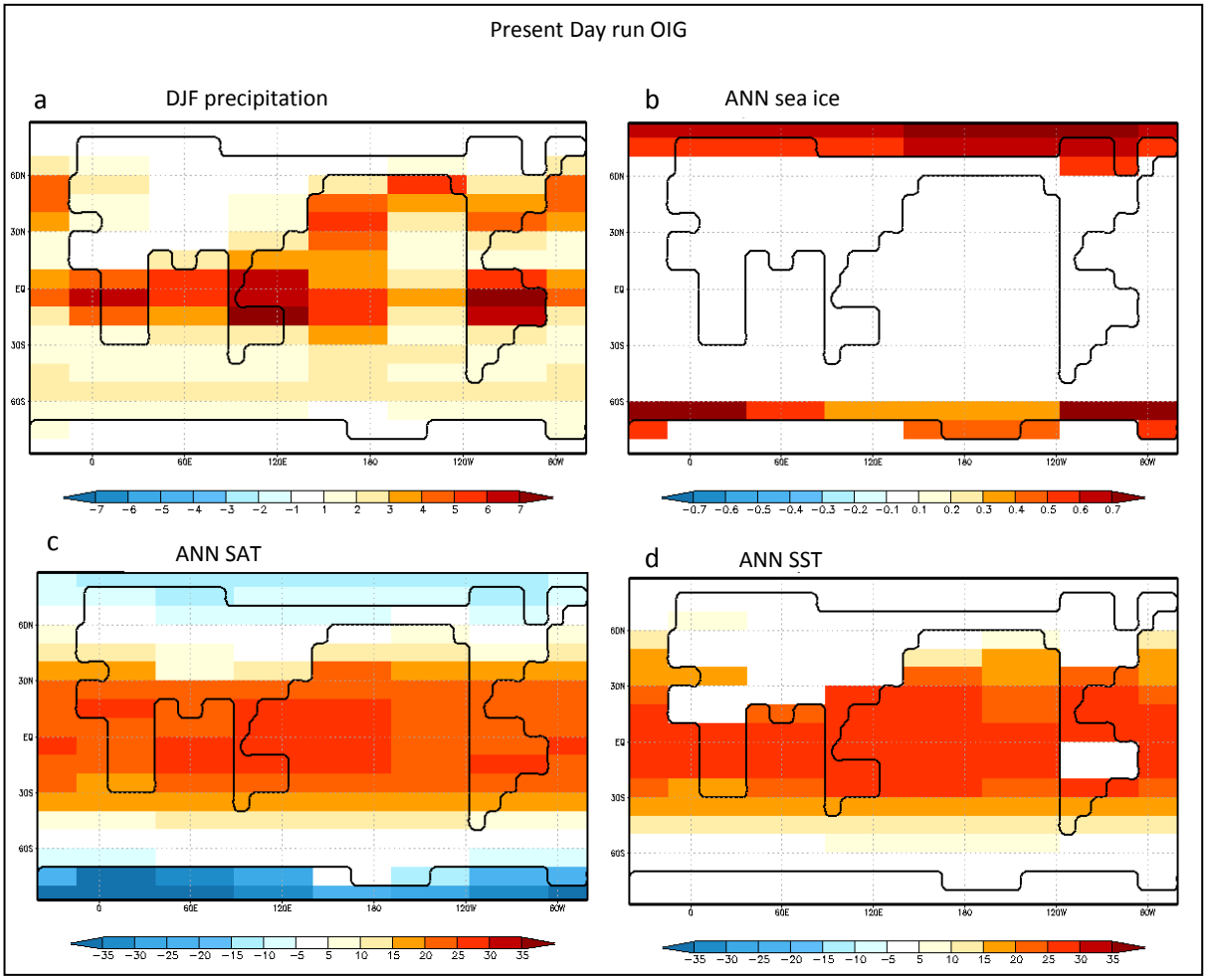

Figure 5: Results for present day for run OIG. (a): Precipitation (mm/day) averaged over December-January-February (DJF), (b): Annual sea ice fraction, (c): Surface air temperature (SAT in degrees Celsius), (d): Sea surface temperature (SST, in degrees Celsius).

To identify the effect of orbital forcing on SH climate, the results for run O during a period with maximum and minimum obliquity (Figure 6) and during periods with minimum and maximum precession (Figure 7) are compared.

The response of precipitation in the SH on obliquity is largest in the low-latitudinal monsoon areas with stronger monsoons during minimum oblquity (Figure 6a). There is a small decrease in sea ice cover during maximum obliquity (Figure 6b). This is in agreement with the higher SAT and SST over the sea-ice covered regions (Figure 6c and 6d, respectively). The SAT shows a small positive difference of 1-2°C at high SH latitudes, i.e. 60°S and higher (Figure 6c). The positive response of the SST is maximum between 50^0S and 60°S and is slightly higer than for SAT (Figure 6d).

The response of the precipitation on precession is very strong at the lower SH latitudes indicating a large increase in monsoon activity during maximum precession. Sea ice fraction, SAT and SST show (almost) no response to precession on the SH (Figure 7).

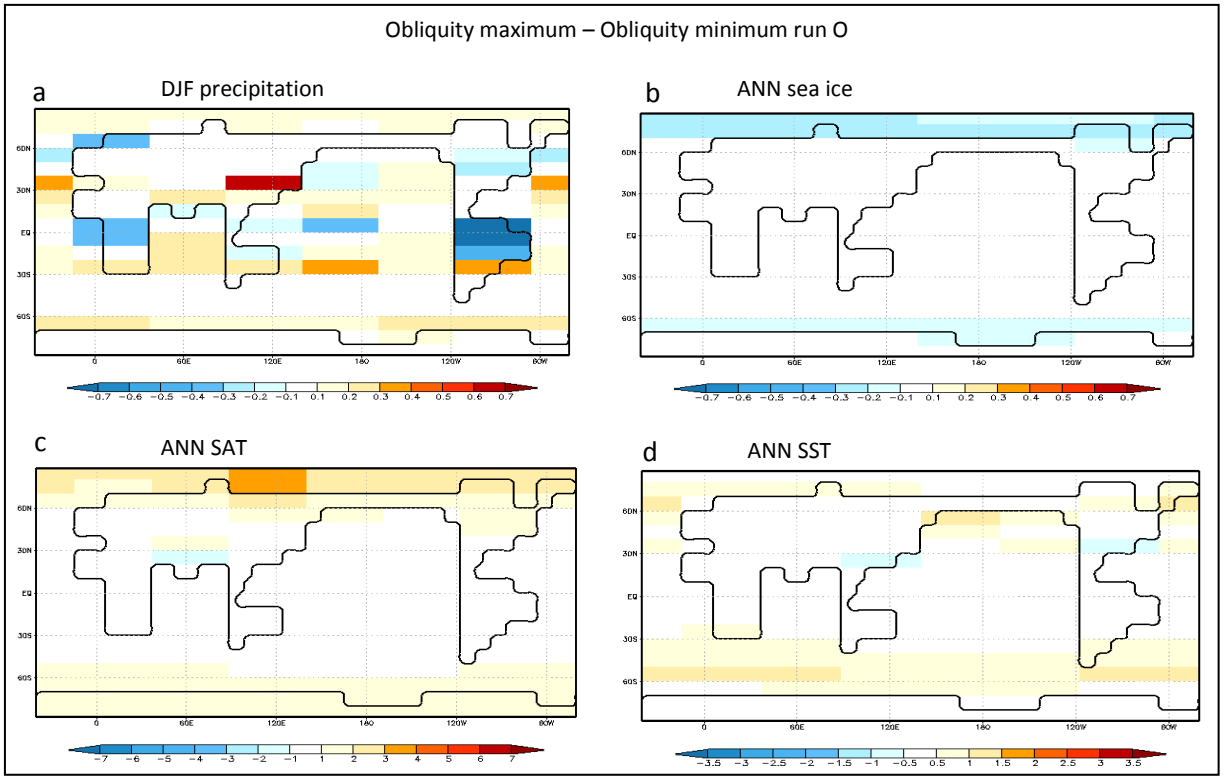

Figure 6: Difference between a period when obliquity is at its maximum (231 kyr BP) minus a period when obliquity is at its minimum (232 kyr BP) of run O. (a): Precipitation (mm/day) averaged over December-January-February (DJF); (b): Annual sea ice fraction; (c): Surface air temperature (SAT in degrees Celsius); (d): Sea surface temperature (SST, in degrees Celsius).

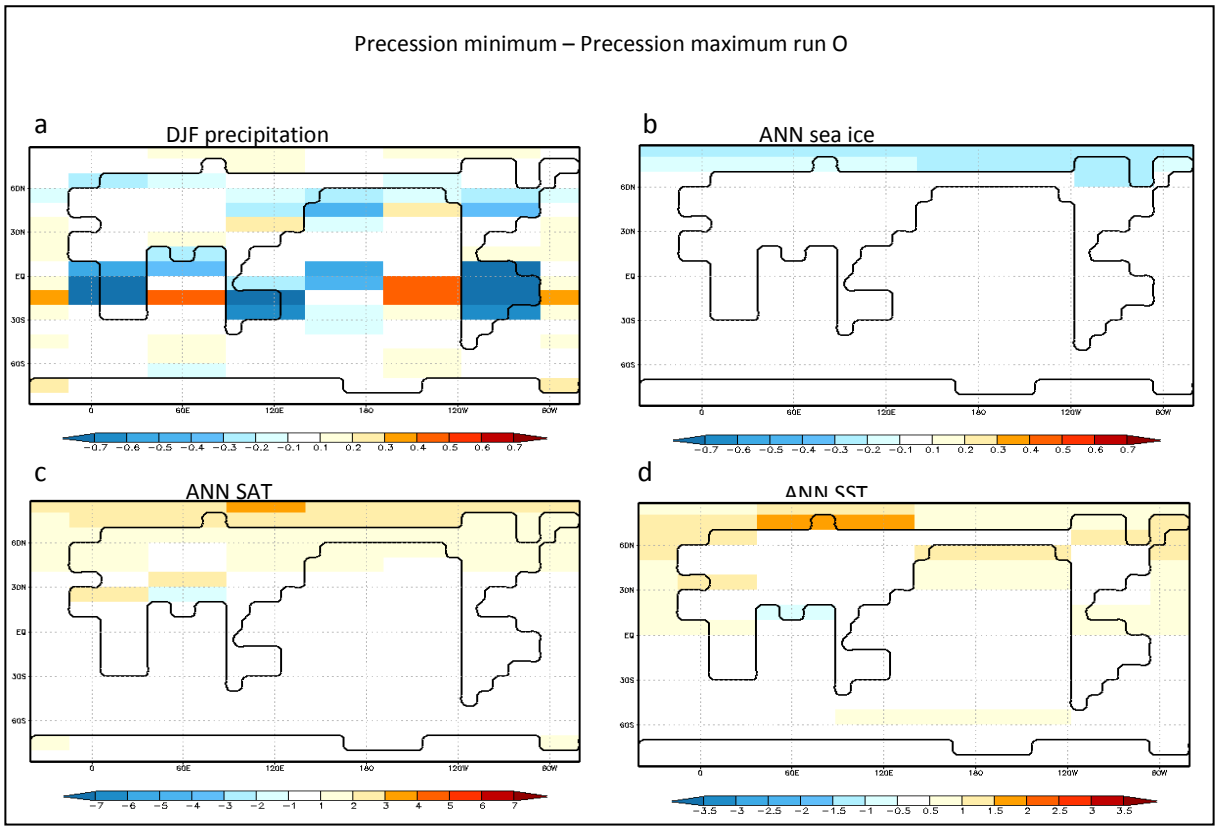

Figure 7: Difference between minimum precession (220 kyr BP) minus maximum precession (210.5 kyr BP). (a): Precipitation (mm/day) averaged over December-January-February (DJF); (b): Annual sea ice fraction; (c): Surface air temperature (SAT in degrees Celsius); (d): Sea surface temperature (SST, in degrees Celsius).

To identify the SH regions where the climate responses to NH ice sheets and GHG forcings are largest, results for OIG during a period with maximum and minimum GHG concentrations (Figure 8) and during periods with minimum and maximum NH ice volume (Figure 9) are compared.
The precipitation response to GHG is largest over the monsoon regions with stronger monsoons during periods with high GHG concentrations (Figure 8a). The SAT shows positive differences over the entire SH (i.e., high temperatures during periods with high GHG concentrations) with the largest amplitude over the high southern latitudes (Figure 8c). The maximum SST response occurs over and near the SH sea-ice covered region with about 3-4 degrees higher temperatures during maximum GHG compared to minimum GHG(Figure 8d). Finally, the sea-ice response is in agreement with the higher SST and SAT, i.e., less sea-ice area during periods with high GHG-concentrations (Figure 8b). Furthermore, during periods with minimum GHG-concentrations the sea-ice coverage extends to 50°S (Figure 8b) while the sea-ice boundary is limited to 60°S when the GHG-concentration is high, e.g. during present-day (Figure 5b).

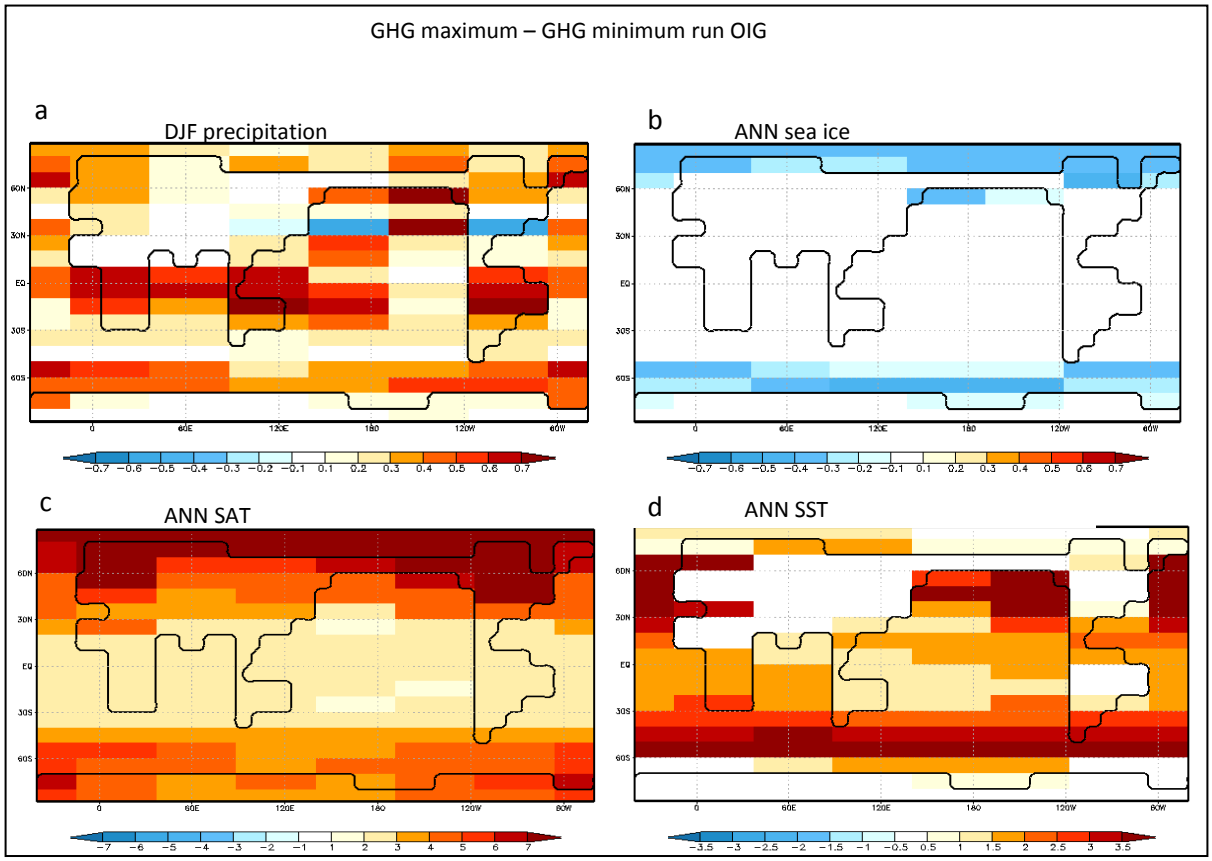

Figure 8: Difference between a period with maximum greenhouse gas concentration (406 kyr BP) minus a period with minimum greenhouse gas concentration (358 kyr BP) of run OIG. (a): Precipitation (mm/day) averaged over December-January-February (DJF); (b): Annual sea ice fraction; (c): Surface air temperature (SAT in degrees Celsius); (d): Sea surface temperature (SST, in degrees Celsius).

The SH climate response to increasing NH ice sheet volumes is very similar to the response to decreasing GHG concentrations, i.e., weaker monsoons, lower temperatures especially over high latitudes and an extending sea-ice coverage during periods with large ice sheet volumes (Figure 9).
For precipitation the areas of interest for further research will be the averaged land covered areas at 15^0S (i.e., the monsoon regions). For SH sea ice the ice fraction will be zonally averaged over the latitudes 55^0S until 75^0S. For SST the areas of further research are the zonal SST over15^0S and 45^0S to

compare mid-latitudinal SST with SST at low latitudes. For SAT the areas of interest are the temperature over land at 15^{0}S to study the influence of the monsoons on air temperature, the zonal SAT over the ocean at 45^{0}S to compare with the SST at the same latitude and the zonal SAT over Antarctica at 85^{0}S.

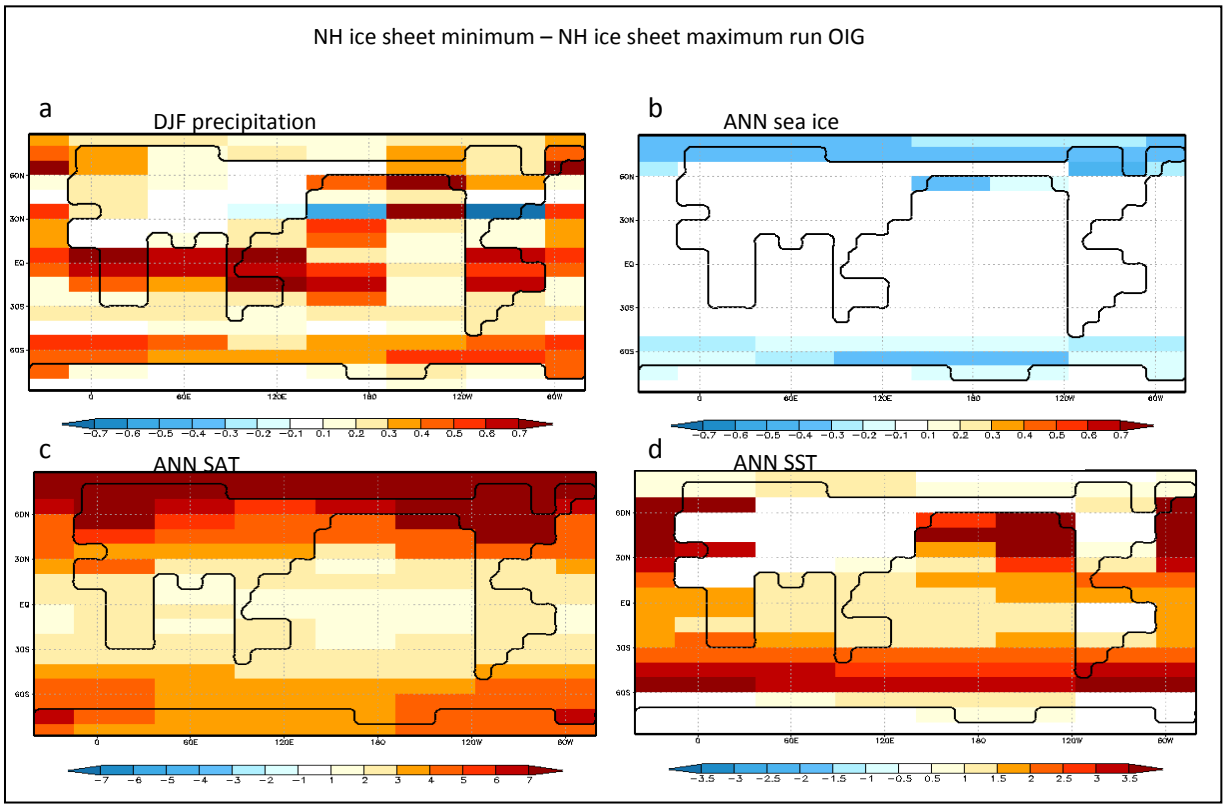

Figure 9: Results of the difference between a minimum northern hemisphere ice sheet volume (405 kyr BP) minus a maximum northern hemisphere ice sheet volume (432.5 kyr BP) of run OIG; (a) Precipitation (mm/day) averaged over December-January-February (DJF) (b): Annual sea ice fraction; (c): Surface air temperature (SAT in degrees Celsius); (d): Sea surface temperature (SST, in degrees Celsius).

3.2 Timeseries

The timeseries of the climate variables for the selected areas are displayed in Figure 10. For precipitation the model simulates no large differences between the runs. There is a small decrease with a maximum of 0.5 mm/day when adding varying ice sheets and/or GHG concentrations, especially in the periods with lower monsoon variations, e.g. around 50 kyr BP (Figure 10a).

The amplitude of the variations in annual SAT due to orbital forcing (run O) are small for 15°S and 45°S (<1^{0}C) and about 1^{0}C for Antarctica (Figure 10c, d and e). In runs OI and OG the amplitudes increase at all latitudes with slightly higher amplitude in run OG compared to run OI. Adding all forcings (run OIG) the amplitudes increase with increasing latitudes: From about 3^{0}C at 15°S via 4^{0}C at 45°S to about 5^{0}C at 85°S.

The temporal behavior of SST is comparable to SAT (Figure 10f and g): Very small amplitude for run O and increasing amplitudes in run OI and OG. At 45°S the amplitude in run OIG for SAT and SST are similar while at 15°S the variations in SST are smaller than for SAT (~2^{0}C and 3^{0}C, respectively).

The timeseries of sea-ice reflect the signal in the SAT and SST. In run O the amplitude is small, it increases in run OI and OG while in run OIG the sea-ice area is about twice as large during cold periods compared to warm periods (Figure 10b).

In summary, in run O the strength of the SH summer monsoons is comparable to run OI, OG and OIG indicating that the summer monsoon is primarily driven by orbital forcing. In contrast, the variations in annual SST, SAT and sea-ice are determined by NH ice sheets and GHG-concentrations with slightly more influence of GHG compared to NH ice sheets.

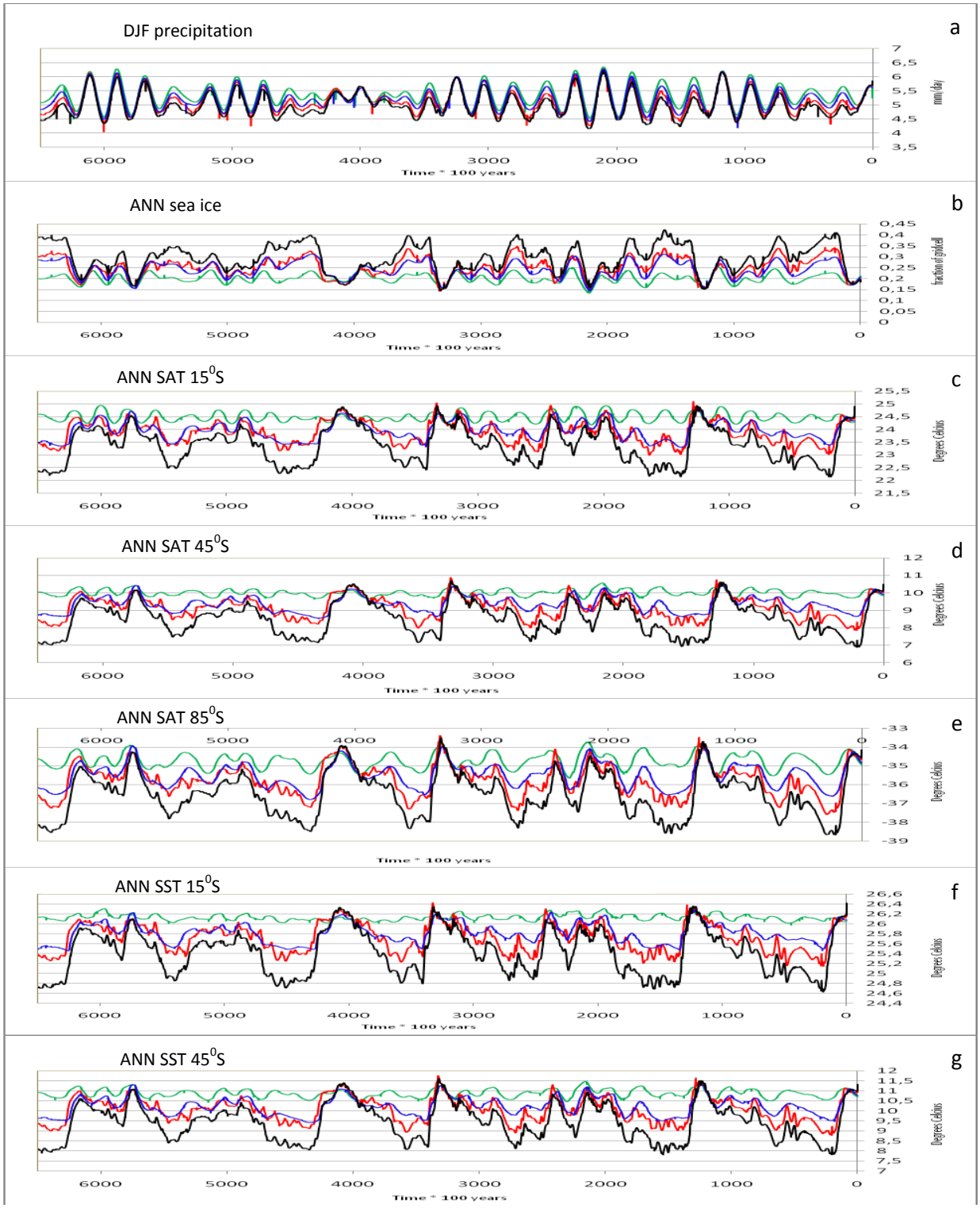

Figure 10: Time series over the last 650 kyr, (a) DJF precipitation in mm/day over land at 15°S; (b), Annual zonal sea ice fraction averaged over 55°S until 75°S; (c), annual SAT over land in degrees Celsius at 15°S; (d), Annual zonal SAT at 45°S; (e) Annual zonal SAT at 85°S; (f) Annual zonal SST in degrees Celsius at 15°S; (g) Annual zonal SST at 45°S..The horizontal axis represents time in 100 years BP. In all figures the green line represents run O, the red line run OG, the blue line run OI and the black line run OIG.

3.3 Spectral analysis

The spectral analyses of the time series are displayed in Figure 11.

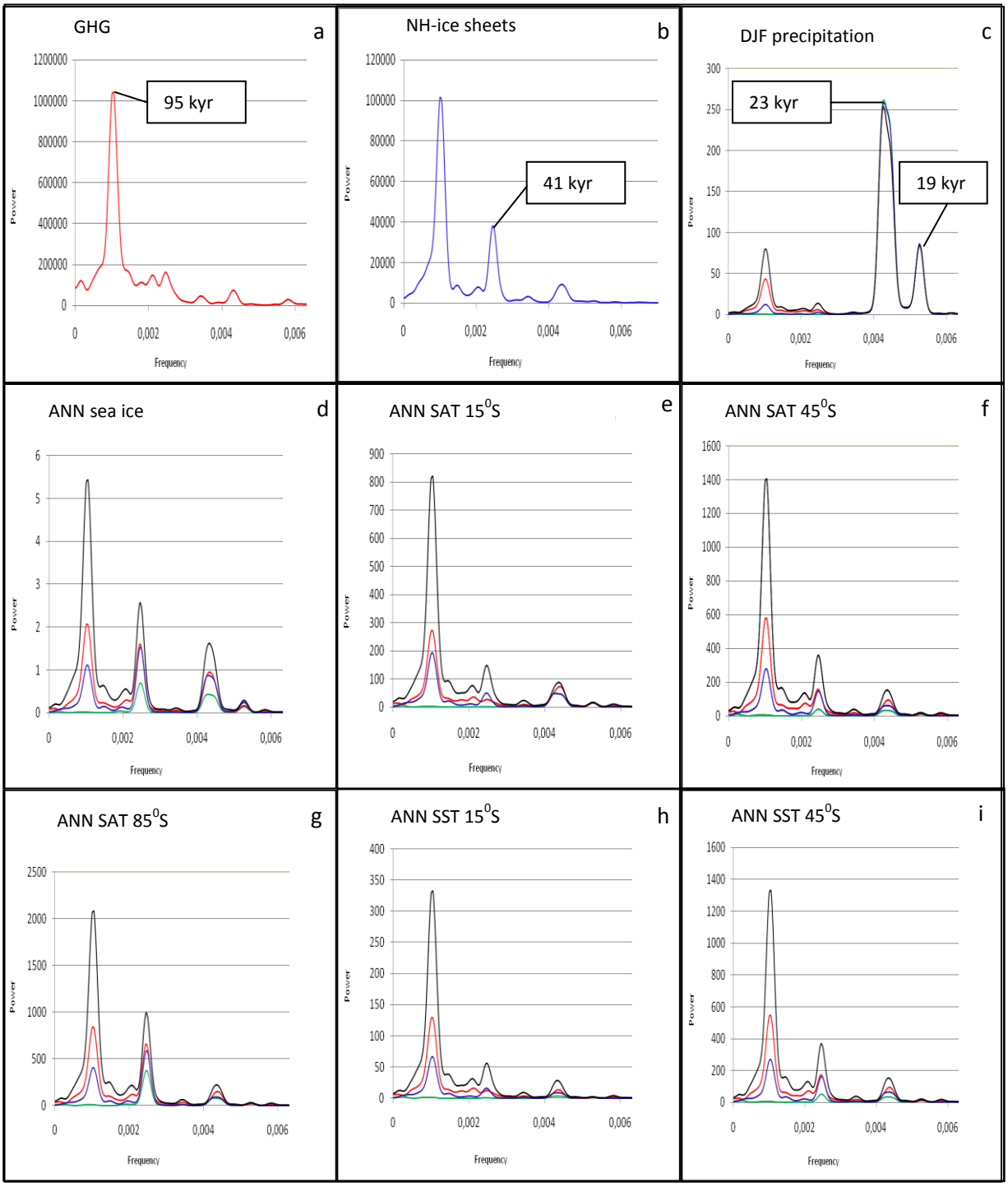

Figure 11: Blackman Tukey spectral analyses of (a) GHG concentrations; (b) ice sheet volumes (c); precipitation in DJF over land at 15°S (d); annual sea ice fraction averaged over 55°S-75°S (e); Annual SAT over land at 15°S (f); Annual SAT at 4°5S; (g) annual SAT over Antarctica at 85°S; (h) annual SST at 15°S; (i) annual SST at 45°S. .The vertical axis represents the power and the horizontal axis the frequency (1/100 years). Lines denote run O (green), run OI (blue), run OG (red) and run OIG (black).

The NH ice-sheets and the GHG-concentrations (Figure 11a and b) show a strong 95 kyr component. In the spectrum of the ice sheet variations there is also an obliquity and a weaker precession component. The GHG-concentrations show a weak obliquity and almost no precession component.
Precipitation spectrum (Figure 11c) due to orbital forcing only (run O), shows a very strong precession (both 23 kyr and 19 kyr peaks) with no obliquity and no 95 kyr component. Adding variable ice sheets (run OI) or GHG-concentrations (run OG) the 95 kyr components is introduced which is stronger in run OG than in OI, while obliquity is very weak in both runs. Adding both forcings (run OIG) increases the power of the 95 kyr component to almost half of the power of precession with a very weak obliquity component.
The spectrum of the sea ice cover (Figure 11d) in run O shows a precession and a stronger obliquity component. In both run OI and OG the power of the obliquity and precession component increases in comparison with run O. Furthermore a 95 kyr component is found, stronger for run OG than OI. In the spectrum of run OIG there is a very strong 95 kyr component that is about twice as strong as the obliquity component and about three times stronger than precession.
SAT in run O shows no spectral power at 95 kyr at all latitudes. At low latitudes the obliquity component is weaker than precession, at mid-latitudes they are comparable while at high latitudes obliquity dominates. In runs OIG, OI and OG the 95 kyr component is strongest except for OI at 85°S where obliquity dominates (Figure 11e, f, and g). Furthermore, spectral power at the 95 kyr band increases going southward. Varying NH ice sheets and GHG result in stronger obliquity and precession at all latitudes compared to run O with a slightly stronger increase in run OG compared to run OI. For all runs except for OIG the power at the precession band is stronger than obliquity at 15°S while at low and mid-latitudes obliquity dominates precession in runs OI, OG and OIG.
The temporal behavior of SST at low and mid-latitudes is comparable to SAT. The only significant difference is the about twice as large spectral power at 15°S for SAT compared to SST (Figure 11h and i).
In summary adding variable ice sheets and/or GHG-concentrations causes a dominant 95 kyr signal in the spectra of the climate responses which is absent in run O. When only adding variable NH ice sheets, obliquity at high latitudes (sea ice cover between 55°S and 75°S and the SAT at 85°S) is the dominant component with a weaker 95 kyr and weak or no precession component. In all of the climate responses except precipitation, adding GHG-concentrations causes a dominant 95 kyr component with increasing power at higher latitudes. In run OIG the power is largest at all dominant periods compared to run O, run OI and run OG.

3.4 Determining leads and/or lags

In Figure 12 the filtered signals of the NH ice sheets and GHG-concentrations are compared with either the filtered precession, the filtered obliquity and to each other in the 95 kyr band to show their leads and/or lags.
The filtered GHG-concentration has a relative low correlation with the filtered precession (-0.67) with a lag of 5.3 kyr (Figure 12a) while the correlation is 0.94 with a lag of 6.2 kyr at the obliquity band (Figure 12b). The ice sheets lag precession by 4.5 kyr with a correlation of 0.94 (Figure 12a) and at the obliquity band there is a 7.1 kyr lag with a correlation of -0.94 (Figure 12b). At the 95 kyr band the GHG-concentrations lead the variable NH ice sheets with 3.5 kyr with a very high negative correlation (-0,99) (Figure 12c).

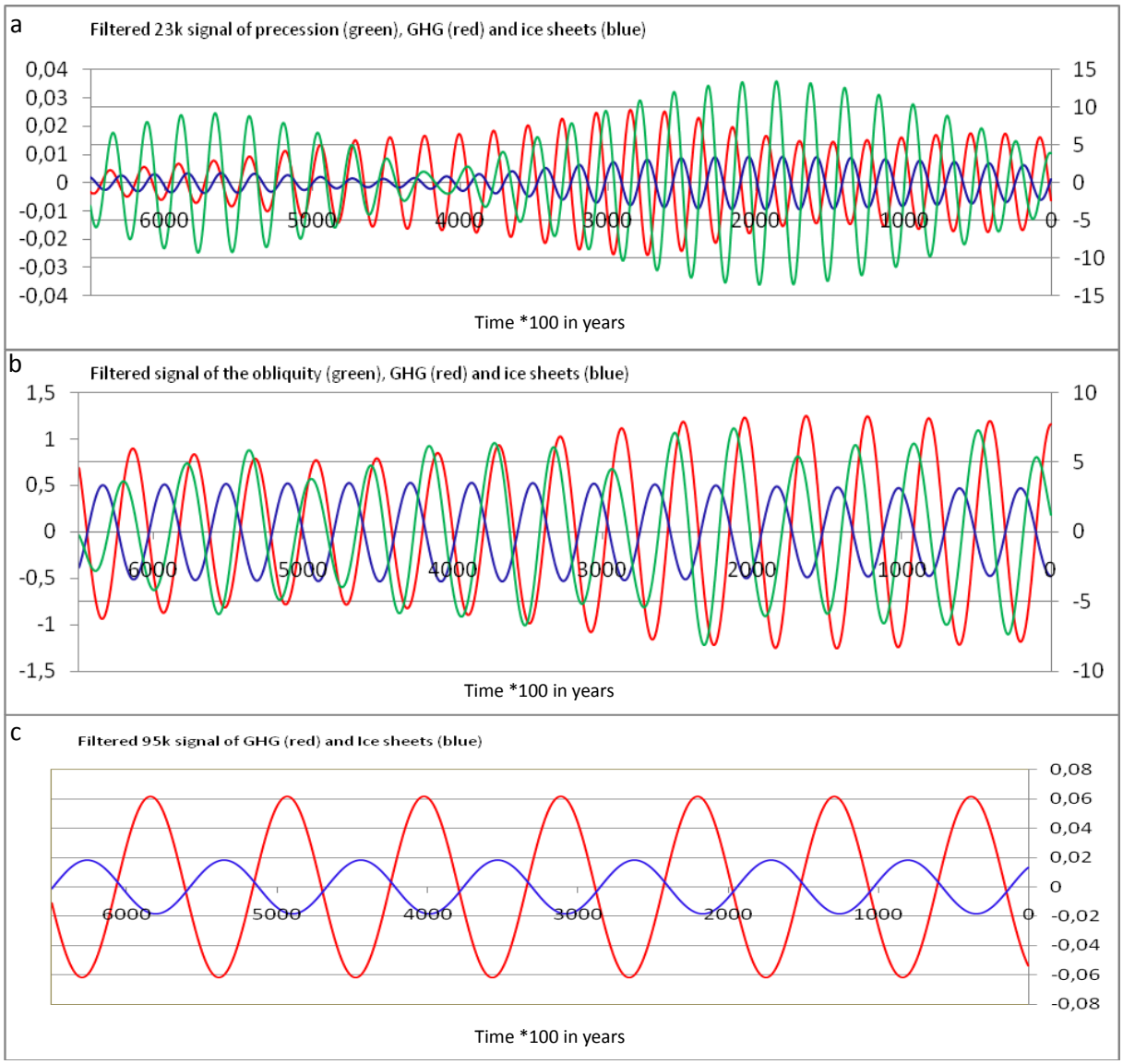

Figure 12: (a) the filtered signals at the 23 kyr band in of the precession parameter (green) the GHG-concentrations (red) and the NH ice sheets (blue); (b) Filtered signals at the 41 kyr band of obliquity (green) the GHG-concentrations (red) and the NH ice sheets (blue); (c) Filtered signals of the GHG-concentrations (red) and the NH ice sheets (blue) at the 95 kyr. The horizontal axis represents time in 100 years BP.

Table 4 shows the leads and lags between the climate variables and precession. The precipitation signal in DJF in run O leads precession by 700 years in run O with a very high positive correlation indicating stronger monsoons during maximum precession. In run OI and OG the lead slightly increases with a maximum increase of 400 years in run OIG.

Sea-ice area increases during maximum precession (i.e., positive correlation) and lags precession by 3.7 kyr in run O. In runs OI and OG the lag significantly increases with for run OI even a longer lag than the lag between ice-sheet volumes and precession.

Although not very strong (Figure 11) a precession signal is found in the time series of SAT at all latitudes. The annual SAT is highest during minimum precession (negative correlation, Table 4), i.e., when the insolation is stronger in SH winter compared to maximum precession. In run O the SAT at 15°S instantaneously responds to the precession forcing while SAT lags precession by about 1 kyr at high and mid-latitudes. In runs OG and OI the lag strongly increases at all latitudes with a slightly

stronger increase for run OI compared to run OG. The combined effect of NH ice-sheets and GHG-concentrations causes the largest lags (run OIG, Table 4).
At mid-latitudes the response time to precession for SST and SAT differ for all runs. At low latitudes the lag for SST is considerably higher compared to SAT in all runs.

GHG	+5300	-0,67						
Ice	+4500	0,94						
	run O	**corr**	**run OG**	**corr**	**run OI**	**corr**	**run OIG**	**corr**
DJF Precip. 15°S	-700	0,99	-900	0,99	-900	0,99	-1100	0,99
ANN Sea-ice	+3700	0,99	+4500	0,97	+4900	0,99	+5100	0,97
ANN SAT 15°S	0	-0,99	+800	-0,95	+1500	-0,99	+2400	-0,94
ANN SAT 45°S	+1200	-0,99	+2600	-0,92	+3400	-0,99	+4000	-0,93
ANN SAT 85°S	+700	-0,99	+2200	-0,92	+3000	-0,99	+3800	-0,93
ANN SST 15°S	+1200	-0,99	+3000	-0,86	+4000	-0,98	+4400	-0,91
ANN SST 45°S	+1400	-0,99	+2600	-0,92	+3500	-0,99	+4100	-0,94

Table 4: Table of the leads and lags in years of the of the filtered climate variables at the precession band. Columns 2, 4, 6 and 8: leads (negative, in years) and lags (positive) of the climate variables and forcings in comparison with the filtered precession signal together with the correlation(r) for run O, run OG, run OI and run OIG. The first two rows show the lags of the filtered GHG-concentrations and the NH-ice sheets on the filtered precession with the correlations (r).

In general, adding varying NH ice-sheets (run OI) or GHG-concentrations (OG) increases the phase difference between climate and precession compared to the orbital forced run (run O). Run OI produces larger lags than run OG, while the lag between the varying GHG-concentrations and precession is larger than that of the variable NH ice sheets and precession. In comparison with the NH ice-sheets the correlation of the GHG-correlations with precession is small. In run OIG the phase differences are largest what is caused by the combination of both variable GHG-concentrations and NH ice-sheets. This indicates that the adding of the NH ice sheets or varying GHG-concentrations slows the response time of the climate variables. While the correlation between the variable GHG-concentrations and precession is low, the correlations of run OG with the precession are high (all higher than +/- 0.92), with the exception of annual SST at 15°S (-0.86).).
Because there is no wheatherlike noise, correlations are near perfect in most of the runs. The results of DJF and JJA show similar responses (increasing leads) and can be found in appendix II.

In Table 5 the lead and lags between the climate variables and obliquity are displayed. Due to a very small response to obliquity, (Figure 11) the phase differences of the climate variables at 15°S were inconclusive and therefore not taken into account.
In contrast to precession (Table 4) where the correlation between the GHG-concentrations and precession was low, the correlation between the varying GHG-concentrations and obliquity is very high with a lag of about 6 kyr (Table 5). The lag between the NH ice-sheet volumes and obliquity (Table 5) is about 2.5 kyr larger than between ice-sheet and precession (Table 4) (i.e., 4.5 kyr and 7.1 kyr).
Sea ice coverage reaches a maximum during minimum obliquity (negative correlations) i.e., when SST and SAT are at a minimum (positive correlations). Both sea-ice and temperatures show similar patterns: The direct lag to obliquity (run O) is very small, i.e., few hundred years, but both varying

GHG-concentrations and NH ice-sheets cause a large increase, stronger for run OI compared to OG. Finally, the combination of GHG and ice-sheets result in the largest lag (run OIG).
The response of the climate to obliquity in December-January-February and June-July-August is similar as the annual response, with either decreasing leads or increasing lags in respectively run OG, OI and OIG (appendix II).

GHG	+6200	0,94						
Ice	+7100	-0,95						
	run O	**corr**	**run OG**	**corr**	**run OI**	**corr**	**run OIG**	**corr**
DJF Precip. 15°S	-	-	-	-	-	-	-	-
ANN Sea-ice	+200	-0,95	+2100	-0,94	+3000	-0,95	+3800	-0,95
ANN SAT 15°S	-	-	**-**	-	-	-	-	-
ANN SAT 45°S	+300	0,95	+3500	0,94	+4800	0,95	+5500	0,95
ANN SAT 85°S	+200	0,95	+2100	0,94	+2800	0,95	+3900	0,95
ANN SST 15°S	-	-	-	-	-	-	-	-
ANN SST 45°S	+300	0,95	+3300	0,94	+4500	0,94	+5200	0,95

Table 5: Table of the leads and lags in years of the of the filtered climate variables at the obliquity band. Columns 2, 4, 6 and 8: leads (negative, in years) and lags (positive) of the climate variables and forcings in comparison with the filtered obliquity signal together with the correlation (r) for run O, run OG, run OI and run OIG. The results for 15S were inconclusive and therefore not taken into account. The first two rows show the lags of the filtered GHG-concentrations and the NH-ice sheets on the filtered obliquity and the correlations.

Table 6 shows the leads and lags between the climate variables and the 95 kyr signal of the GHG-concentrations or the NH ice-sheets.
The GHG concentrations lead the NH ice-sheets by 3.5 kyr. For all climate variables and all runs the correlations are very close to 1 or -1. When run OG is compared with the varying GHG-concentrations at the 95 kyr band, there are almost no lags, i.e. the climate variables are in phase with the GHG-concentrations. In run OI Climber simulates leading climate variables compared to the NH ice-sheets with phase differences between 1.3 and 2.2 kyr. Comparing the 95 kyr filtered variables in run OIG with the GHG-concentrations, lags are found between 700 years and 1500 years. Compared to the ice sheet volumes all leads vary between 2000 and 2800 years. Climber simulates the same response for DJF and JJA and these tables can be found in the appendix II.

GHG	**-3500**	**-0,99**						
	run OG	**corr**	**run OI**	**corr**	**run OIG wrt. GHG**	**corr**	**run OIG wrt, Ice**	**corr**
DJF Precip. 15°S	+200	0,99	-2200	-0,99	+700	1	-2800	-1
ANN sea-ice	+400	-0,99	-1300	1	+1500	-1	-2000	0,99
ANN SAT 15°S	+500	0,99	-1300	-1	+1200	0,99	-2300	-1
ANN SAT 45°S	0	0,99	-1800	-1	+1100	0,99	-2400	-1
ANN SAT 85°S	0	0,99	-1400	-1	+1400	0,99	-2100	-1
ANN SST 15°S	+500	0,99	-1800	-0,99	+1000	0,99	-2500	-0,99
ANN SST 45°S	+600	0,99	-1800	-0.99	+1100	0,99	-2400	-0,99

Table 6: Table of the leads and lags in years of the of the filtered climate variables at the 95 kyr band. Run OG and OIG are compared to the 95 kyr signal of the GHG-concentrations (column 2 and 6) and OI and OIG compared to the 95 kyr signal of the NH ice sheets (column 4 and 8) with the correlations (r) (column 3, 5, 7, 9). The first row shows the lead of the filtered GHG-concentrations on the filtered NH-ice sheets with the correlation.

3.5 Deuterium

In Figure 13 the timeseries of deuterium is shown. It shows many similarities with the SAT at 85°S.

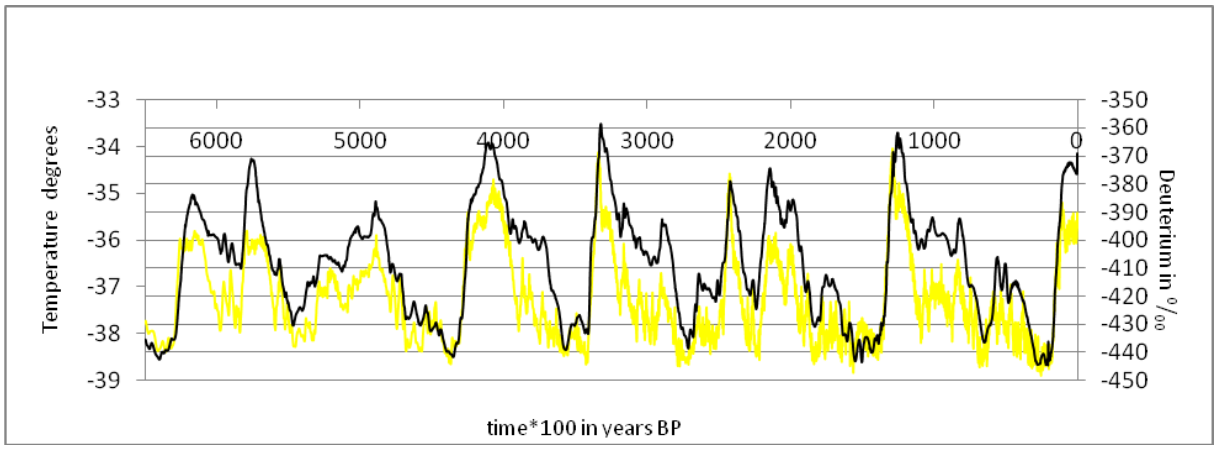

Figure 13: Timeseries for Deuterium (yellow) in $^{0}/_{00}$ from the Epica dome C (EDC) and SAT 85°S (black) in °C run OIG from 650 kyr BP until present-day. The horizontal axis shows time in 100 years BP.

To analyze the dominant factors in the timeseries the results of the spectral analysis can be found in Figure 14. Deuterium shows a strong ~95 kyr component with a weaker obliquity and weak precession. The ratios between the powers of the dominant periods in the Deuterium records are closest to the ratios in run OIG compared to the other runs. This indicates that the correlation between the simulated annual SAT at 85°S and the deuterium record is higher for run OIG compared to the other runs.

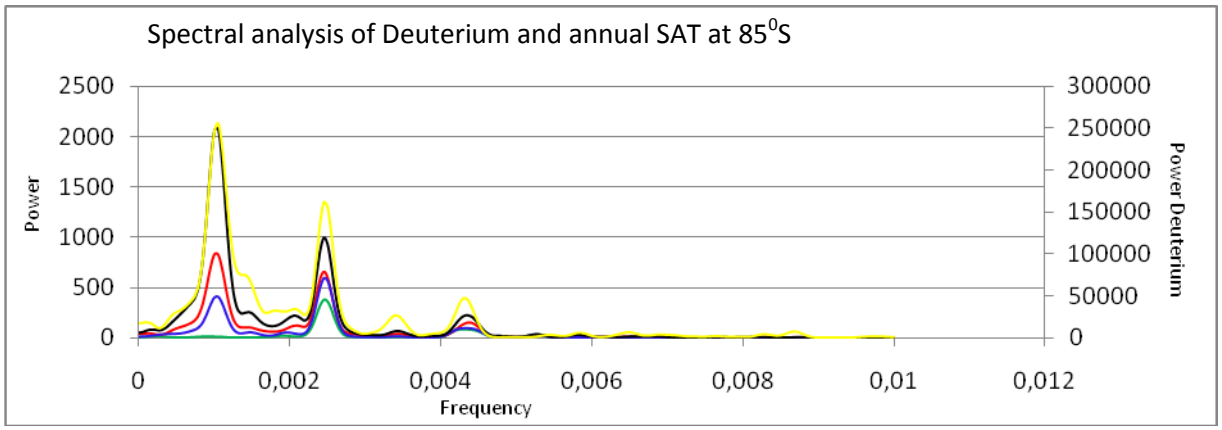

Figure 14: Blackman Tukey spectral analyses of Deuterium record (yellow) Annual SAT at 85^{0}S for run O (green), run OG (red), run OI (blue) and run OIG (black). The y axis represents the power and the x axis the frequency.

This is also confirmed by the computed correlations between deuterium and the (filtered) annual SAT at 85°S for all runs (Table 7). Because of the small power of precession there is no comparison between filtered signals at this period.

	Run O	Run OG	Run OI	Run OIG
Timeseries	0.40	0.88	0.73	0.87
Filter obliquity	0.77	0.92	0.96	0.99
Filter 95 kyr	-	0.97	0.94	0.96

Table 7: Correlations between respectively the timeseries of deuterium and the timeseries (run O, run OG, run OI and run OIG) of the SAT at 85^0S. In the second row the correlations between the filtered deuterium and the filtered obliquity signals of the runs are shown, and the last row shows the correlations between the filtered deuterium and the annual SAT at 85S at the 95 kyr.

In general the correlations for the (un)filtered timeseries for the annual SAT at 85°S and deuterium are highest for run OIG. The correlations for run OG are comparable to run OIG with slightly lower correlations for run OI and significantly lower correlation for run O.

4. Discussion

The results of the leads and lags are computed using the timeseries of the ice-sheet volumes and GHG-concentrations. Therefore due to uncertainties in the age models used for tuning these records, there are also uncertainties in the estimated phase differences (Mudelsee, 2001; Weber and Tuenter, 2011).

An important caveat in the present study is the absence of the fresh water fluxes, i.e. the runoff during the waning of the NH ice-sheets and the fresh water transport from the oceans to the continents during the waxing of the ice-sheets. These perturbations in fresh water fluxes have a large effect on the Thermohaline circulation that is considered to be an important factor in linking the NH with the SH climate variables (Imbrie et al. 1989; Lohman et al. 1996; Couch and Eyles, 2008; Stocker, 2000). Another uncertainty is the fixed ice-sheet volume of Antarctica in all runs. Although the variations in Antarctic ice-sheet volume were much smaller than the volume changes of the NH ice sheets during the last 650 kyr, they could have influenced SH climate, especially at high latitudes. Additional simulations with a changing Antarctic ice-sheet are needed to identify the role of the Antarctica in SH climate variations.

In the current study a 95 kyr period is found that in literature often is referred to as 100 kyr period originating from eccentricity (Ruddiman, 2003). However, the spectral analysis of eccentricity reveals that the main period is 100 kyr or even somewhat longer while the dominant period in GHG-concentrations and ice-sheet volumes is 95 kyr. Some studies suggest that this 95 kyr period can be explained by multiples of obliquity or precession cycles while others propose an interplay of precession cycles and obliquity cycles with considerations of total energy input and threshold effects (Huybers and Wunsch, 2005; Huybers, 2006; Raymo et al., 2006) . However, it is beyond the scope of the current study to explain the origin of the 100/95 kyr cycle in climate.

At the period of precession there are small changes in the timing of the monsoon in DJF, i.e. the monsoon leads precession by about 700 years in run O. This lead reflects the response of the DJF precipitation to the insolation during November-December-January caused by thermal inertia as also found for the NH summer monsoons (Tuenter 2004).

Comparing the response of the SH summer monsoons with that of the NH summer monsoons (Weber and Tuenter, 2011), differences can be seen. The SH precipitation in run O leads precession with a few hundred years in agreement with the 400 years for the NH. However, in run OIG the lead significantly increases (1.1 kyr) on the SH while on the NH the phase difference is negligible (Weber and Tuenter, 2011). This indicates that at the precession band the influence of GHG and/or NH ice-sheets on the SH summer monsoon is stronger than on the NH summer monsoon. In contrast, at the obliquity band there was no significant signal found in the results of the SH monsoons while the obliquity signal in the NH monsoons were found both in proxy data and in the modeling studies (Clemens and Prell, 2003; Tuenter et al, 2005; Clemens and Prell 2006; Weber and Tuenter, 2011). This could be explained by the absence of large land areas on the SH that can transfer the obliquity signal from high latitudes to the low latitudinal monsoons as was found for the NH (Chen et al, 2011; Tuenter 2004; Weber and Tuenter, 2011).

Because precession has no net annual signal, in the results of the annual climate variables there is (almost) no precession signal found. Because seasonal the precession (and less for obliquity) signal is very strong, in the results of the seasonal precipitation the precession signal is very dominant. This was also concluded by Weber and Tuenter 2011 in relation to the NH monsoon responses.

At low latitudes, the results for obliquity were also inconclusive for SAT and SST. This indicates that there is no transfer of the obliquity signal from the high SH latitudes to low SH latitudes but also that interhemispheric linkages at the obliquity band are not likely for the low latitudes on the SH.

At the precession band sea-ice is in phase with the NH ice sheets, indicating a fast teleconnection via the atmosphere from the NH to the SH. For the obliquity and 95 kyr band the sea ice cover shows similar responses as SST and SAT, respectively leading NH ice-sheets by 3 kyr in OI to 5 kyr in OIG at the obliquity band and from 2 kyr in run OI to 3 kyr in run OIG at the 95 kyr band. Renssen et al. (2005) suggested for the climate in the Holocene that local insolation forcing and the long term memory of the system explain the responses on the SH-climate to a large extent with sea ice as a strong amplifying factor due to the Albedo effect. Furthermore the research of Denis et al. (2010) also shows a strong relation between the insolation differences at the SH and the responses of the SH-climate in the Holocene. Increasing insolation is responsible for oceanic and cryospheric feedbacks affecting the latitudinal thermal gradient. These studies could explain why the response of the sea-ice to the forcings is similar as the responses of SST and SAT.

The only period that is introduced by adding GHG-concentrations and NH ice-sheets is 95 kyr. Comparing climate in run OG is to the 95 kyr component in the GHG-concentrations, the phase differences are very small i.e. the climate variables are in phase with the GHG-concentrations. On the other hand, the 95 kyr band of the climate on the SH leads the NH ice-sheets by ~1.5 kyr. Other studies also identified leads of the SH climate compared to the NH ice-sheets (Shulmeister et al., 2006; Yin et al, 2009). Crundwell et al. (2008) also found that the SST at ~45^0S leads the NH ice sheets and explained this by tropical forcings of the southern mid-latitude ocean climate during de-glacial warming. This suggests that the Tropics might play an important role in the transfer of glacial signals from the NH to the SH. Further research is needed to verify this.

There are many similarities found in the Deuterium record form Antarctica and the modeling results. It is found that orbital forcing alone is not sufficient to explain the Antarctic temperature and that both NH ice-sheets and greenhouse gas concentrations are necessary where the influence of the GHG-concentrations is larger the influence of the NH ice-sheets. This is in agreement with Jouzel (2007) who also points to a strong carbon-cycle feedback involved in the magnitude and durations of the glacials and therefore to the global character of the Antarctic deuterium record.

5. Conclusions

Long transient run for the last 650,000 years are used to assess the impact of orbital forcing, varying GHG-concentrations and NH ice sheets on the Southern Hemisphere climate.

The influence of orbital forcing on the SH low-latitudinal monsoonal summer precipitation dominates the influence of varying GHG-concentrations and NH ice-sheets. For the SH monsoons the obliquity signal is not found in contrast with the NH monsoons where obliquity is found both in proxy data and modeling studies.

The influence of NH ice-sheets and GHG-concentration on SST, SAT and sea-ice is larger than the direct influence of orbital forcing, especially at high latitudes. At low latitudes temperatures are equally affected by varying GHG-concentrations and NH ice-sheets while at high latitudes GHG-concentrations become the dominant forcing.

If climate is only forced by orbital induced insolation changes the variability is dominated by obliquity and precession, with no obliquity component at the low SH latitudes and an increasing strength going to high latitudes. Adding varying GHG-concentrations and/or NH ice sheets, a 95 kyr component is introduced. For the monsoonal precipitation precession is still the dominant component when adding varying GHG-concentrations and/or NH ice-sheets. If only adding variable NH ice sheets, obliquity is still the dominant component with a weaker 95 kyr and weak or no precession component. In contrast for SST, SAT and sea-ice , adding GHG-concentrations causes a dominant 95 kyr component with increasing power at higher latitudes. The combined orbital forcing, GHG-concentrations and NH ice-sheets (run OIG) leads to the strongest dominant periods (with an exception for precipitation) compared to a single forcing or a combination of two forcings.

At the precession band, adding NH ice sheets or varying GHG-concentrations increases the response time of all studied climate variables significantly, with the exception of precipitation that is, as concluded earlier, primarily driven by the orbital forcing. In general, run OI produces larger lags than run OG, caused by the stronger precession component found in the NH ice-sheets in comparison with the precession component found in GHG-concentrations. Adding both in run OIG produces the largest lags for precession.

At the obliquity band all climate variables at mid- and high latitudes respond similar in proportion to the lags between the forcings and obliquity. The response to obliquity of the temperature over Antarctica is faster than the response of the SST and the SAT at mid SH latitudes.

At the 95 kyr band the GHG-concentrations lead the NH ice sheets by 3.5 kyr. Due to the dominance of the GHG-concentrations, SH climate leads the NH-ice sheets with 2-3 kyr in run OIG.

The results of the Deuterium showed that orbital forcing alone is not sufficient to explain the Antarctic temperature and that both NH ice-sheets and greenhouse gas concentrations are necessary where the influence of the GHG-concentrations is larger the influence of the NH ice-sheets.

In summary, the orbital forcings are dominant for the (seasonal) monsoonal precipitation on the SH while annual sea-ice, SAT and SST are primarily forced by the GHG-concentrations and the NH ice-sheets. The results show that in general the GHG-concentrations are the dominant factor, especially at the higher SH latitudes, but the NH ice-sheets still play an important role (more in the lower SH latitudes) in the SH climate responses.

To further understand SH climate on orbital timescales the first step is to obtain more sedimentary records from the SH that are sufficiently long to identify orbital induced climate variations. Secondly the modeled connection between the NH and SH via the Thermohaline circulation probably will be

more accurate when fresh water fluxes caused by the waxing and waning of NH ice-sheets will be included. Thirdly, the simulated SH climate could improve if glacial variations of the Antarctic ice-sheet are included. Finally, in the near future it hopefully will be possible to make very long transient runs with more detailed models without having such long computation times. Because Earth's climate is very complicated this will certainly result in more realistic climate simulations on orbital timescales.

References

Berger, A.L., Loutre, M.F., Tricot, C., 1993. Insolations and Earth's orbital periods.Journal of Geophisical Research, Volume 98 (D6), pp 10,341-10,362.

Broccoli A.J., Manabe, S., 1987. The Influence of Continental Ice, Atmospheric CO_2 and Land Albedo on the Climate if the Last Glacial Maximum. Climate Dynamics, Volume 1, pp 87-99.

Chen, G.S., Liu, Z., Clemens, S.C., 2011. Modeling the time-dependent response of the Asian summer Monsoon to obliquity forcing in a coupled GCM: a PHASEMAP sensitivity experiment. Climate Dynamics, Volume 36, pp 695-710.

Clemens, S.C., Prell, W.L., 2003. A 350,000 year summer monsoon multi-proxy stack from Owen Ridge, Northern Arabian Sea. Marine Geology, Volume 201, pp 35-51.

Clemens, S.C., Prell, W.L., 2007. The timing of the orbital-scale Indian monsoon changes. Quaternary Science Reviews, Volume 26, pp 275-278.

Clemens, S.C., Prell, W.L., Sun, Y., 2010. Orbital-scale timing and mechanisms driving late Pleistocene Indo-Asian summer monsoons: reinterpreting cave speleothem d18O. Paleoceanography 25, PA4207. doi:10.1029/2010PA001926.

Couch, A.G., Eyles, N., 2008. Sedimentary record of glacial Lake Mackenzie, Northwest Territories, Canada: Implications for Arctic freshwater forcing. Palaeogeography, Palaeoclimatology, Palaeoecology, Volume 268, pp 26-28.

Crucifix, M., Loutre, M.F., Berger, A., 2006. The climate response to astronomical forcing. Space Science Reviews, Volume 125, pp 213-226.

Crundwell, M., Scott, G., Carter, L., 2008. Glacial-Interglacial Ocean Variability form Planktonic Foraminifera during the Mid-Pleistocene transition in the Temperate Southwest Pacific, ODP Site 1123. Palaeogeography, Palaeoclimatology, Palaeoecology. Volume 260, pp 202-229.

Denis, D., Crosta, X., Barbara, L., Massé, G., Renssen, H., Ther, O., Giraudeau, J., 2010. Quaternary Science Reviews, Volume 29, pp 3709-3719.

Ganopolski, A., Rahmstorf, S., Petoukhov, G., Claussen, M., 1998a. Simulations of Modern and Glacial Climates with a Coupled Model of Intermediate Complexity. Nature, Volume 391, pp 351-356

Ganopolski, A., Kubatzki, C., Claussen , M., Brovkin, V., Petoukhov, G., 1998b. The Influence of Vegetation-Atmosphere-Ocean Interaction on Climate Druring the Mid-Holocene. Science, Volume 280, pp1916-1919.

Ganopolski, A., Roche M.D., 2009. In the Nature of Lead-Lag Relationship during Glacial- Interglacial Climate Transitions. Quaternary Science Reviews, Volume 28, pp 3361-3378.

Hargreaves, J.C., Abe-Ouchi, A., 2003. Timing of ice-age terminations determined by wavelet methods. Paleoceanography, Volume 19 (2), 1035.

Hays, J.D., Imbrie, J., Shackleton, N.J., 1976. Variations in the Earth's Orbit: Pacemaker of the Ice Ages. Science, Volume 194, Number 4270, pp 1121-1132.

Huybers, P., 2006. Early Pleistocene Glacial Cycles and the Integrated Summer Insolation Forcing.; Science, Volume 313 (5786), pp508-511.

Huybers, P., Wunch, C., 2006. Obliquity pacing of the late Pleistocene glacial terminations. Nature, Volume 434 (7032), pp 491-494.

Imbrie, J., Imbrie, K.P., 1979. Ice Ages; Solving the Mystery. The Macmillan Press LTD. London, England. pp 161-176

Imbrie, J., McIntyre, A., Mix, A., 1989. Oceanic Response to Orbital Forcing in the Late Quarternary: Observational and Experimental Strategies. In: Berger, A.L. et al. (Eds), Climate and Geoscienses. Kluwer Academic Publications., Dordrecht, pp 121-164.

Jouzel, J., 2004. EPICA Dome C Ice Cores Deuterium Data. IGBP PAGES, World Data Center for

Paleoclimatology, Data Contribution Series # 2004 - 038. NOAA/NGDC Paleoclimatology Program, Boulder CO, USA. doi: 10.3334/CDIAC/cli.007

Jouzel, J., V. Masson-Delmotte, O. Cattani, G. Dreyfus, S. Falourd, G. Hoffmann, B. Minster, J. Nouet, J.M. Barnola, J. Chappellaz, H. Fischer, J.C. Gallet, S. Johnsen, M. Leuenberger, L. Loulergue, D. Luethi, H. Oerter,F. Parrenin, G. Raisbeck, D. Raynaud, A. Schilt, J. Schwander, E. Selmo, R. Souchez, R. Spahni, B. Stauffer, J.P. Steffensen, B. Stenni, T.F. Stocker, J.L. Tison, M. Werner, and E.W. Wolff.,2007. Orbital and Millennial Antarctic Climate Variability over the Past 800,000 Years. Science, Volume 317(5839), pp.793-797.

Kutzbach, J.E., Liu, X., Liu, Z., Chen, G., 2008. Simulation of the evolutionary response of global summer Monsoons to orbital forcing over the past 280,000 years. Climate Dynamics, Volume 30, pp 567-579.

Laskar, J., Robutel, P., Joutel, F., Gastineau, M., Correia, A.C.M., Levrand, B., 2004. A Long Term Numerical Solution for the Insolation Quantities. Astronomy and Astrophysics, Volume 428, pp 261- 285.

Lohmann, G., Gerdes, R., Chen, D., 1996. Sensitivity of Thermohaline circulation in coupled oceanic GCM – Atmospheric GBM experiments. Climate Dynamics, Volume 12, pp 403-416

Loulergue, L., Schilt, A., Spahni, R., Masson-Delmotte, V., Blunier, T., Lemieux, B., Barnola, J.-M., Raynaud, D., Stocker, T.F., Chappellaz, J., 2008. Orbital and millennial-scale features of atmospheric CH4 over the past 800,000 years. Nature, Volume 453, pp 383-386. doi:10.1038/nature06950.

Lüthi, D., Le Floch, M., Bereiter, B., Blunier, T., Barnola, J.-M., Siegenthaler, U., Raynaud, D., Jouzel, J., Fischer, H., Kawamura, K., Stocker, T.F., 2008. High resolution carbon dioxide concentration record 650,000e800,000 years before present. Nature, Volume 453, pp 379-382. doi:10.1038/nature06949.

Mudelsee, M., 2001. The phase relations among atmospheric CO_2 content, temperature and global ice volume over the past 420 ka. Quaternary Science Reviews, Volume 20, pp 583-589.

Nelson, C. S., Hendy, C. H., Jarrett, G. R., and Cuthbertson, A. M., 2 1985. Near-synchronicity of New Zealand alpine glaciations and Northern Hemisphere continental glaciations during the past 750 kyr. Nature, Volume 318, pp 361–363

Paillard, D., 2001. Glacial cycles: Towards a new paradigm. Review of Geophysics, Volume 39 (3), pp 325-346.

Paillard, D., Labeyrie, L., Yiou, P., 1996. Macintosh program performs time series analysis. EOS 77, 379.

Peltier, W.R., 2004. Global glacial isostasy and the surface of the ice-age earth: the ICE-5G (VM2) model and GRACE. Annual Review of Earth and Planetary Sciences, Volume 32, pp 111-149.

Petoukhov, V., Ganopolski, A., Brovkin, V., Claussen, M., Eliseev, A., Kubatzki, C., Rahmstorf, S., 2000. CLIMBER-2: a Climate Model of Intermediate Complexity. Part 1: Model Description and Performance for Present Climate. Climate Dynamics, Volume 16, pp 1-17.

Raymo, M., Nisancioglu, K., Lisiecki, L., 2006. Plio-Pleistocene Ice Volume, Antarctic Climate, and the Global δ18O Record. Science, Volume 313(5786), pp 492-495

Renssen, H., Goosse, H., Fichefeti, T., Masson-Delmonte, V., Koç, N., 2005. Holocene climate evolution in the high-latitude Southern Hemisphere simulated by a coupled atmosphere-sea-ice-ocean-vegetation model. The Holocene, Volume 15, pp 951-964.

Ruddiman, W.F., 2003. Orbital Insolation, Ice Volume and Greenhouse Gases. Quaternary Science Reviews, Volume 22, pp 3092-3112.

Ruddiman, W.F., 2006. Orbital Change and Climate. Quaternary Science Reviews, Volume 25, pp 3092-3112.

Ruddiman, W.F., 2008. Earth's Climate, Past and Future, Second Edition. W.H. Freeman and Company, New York.

Shulmeister, J., Rodbell, D.T., Gagan, M.K., Seltzer, G.O., 2006. Inter-Hemispheric Linkages in Climate Change: Paleo-Perspectives for Future Climate Change. Climate of the Past Discussions. Volume 2, pp 79-122.

Stenni, B., Jouzel, J., Masson-Delmotte, V., Castellanoc, E., Cattani, O., Falourd, S., Johnsen, S. J., Longinelli, A., R¨othlisberger, R., Sachsi, J. P., Selmo, E., Souchez, R., Steffensen, J. P., and Udisti, R. 2003. A high resolution site and source late glacial temperature record derived from the EPICA Dome C isotope records (East Antarctica), Earth Planetary Science Letters, Volume 217, pp 183–195,

Stocker, T. F., **2000.** Past and future reorganizations in the Climate System, Quaternary. Science. Reviews, Volume 19, pp 301–319.

Tuenter, E., 2004. Modeling Orbital Induced Variations in Circum-Mediterranean Climate. University Utrecht, Utrecht.

Waelbroeck, C., Jouzel, J., Labeyrie, L., Lorius, C., Labracherie, M., Stievenard, M., Barkov, N.I., 1995. A comparison of the Vostok ice Deuterium record and series from Southern Ocean core MD 88/770 over the last two glacial-interglacial cycles. Climate dynamics, Volume 12, pp 113-123.

Weber, S.L., Tuenter, E., 2011. The impact of varying ice sheets and greenhouse gases in the intensity and timing of the boreal summer monsoons. Quaternary Science Reviews, Volume 30, pp 469-479.

Weirt, S., 2008. Past Cycles, Ice Age Speculations. As essay in: Discovery of Global Warming. Spencer Weart & American Institute of Physics. Harvard University Press. Cambridge, Massachusetts, USA.

Yin, Q.Z., Berger, A., Crucifix, M., 2009. Individual and combined effects of ice sheets and precession on mis-13 climate. Climate of the Past, Volume 5 (2), pp 229-243.

Ziegler, M., Lourens, L.J., Tuenter, E., Hilgen, F., Reichart, G.-J., Weber, S.L., 2010. Precession phasing offset between Indian summer monsoon and Arabian Sea productivity linked to changes in Atlantic overturning circulation. Paleoceanography 25, PA3213. doi:10.1029/2009PA001884.

Appendix I

For all the different inputs according Table 1 the following data is available:

tsur	15	99	TSURA	- surface temperature (SST/land)	[C]	1
ts	15	99	TASURA	- surface air temperature	[C]	2
t850	15	99	T850	- air temperature 850 mb	[C]	3
t200	15	99	T200	- air temperature 200 mb	[C]	4
gam	15	99	GAM	- lapse rate	[K/m]	5
htrop	15	99	HTROP	- tropopaus height	[m]	6
conv	15	99	CONVTMP	- energy convergence	[W/m^2]	7
tam	15	99	TAM	- effective atmosphere tempr	[C]	8
tsl	15	99	TSL	- sea surface temperature	[C]	9
fs1	15	99	FSW1	- solar flux at the surface	[W/m^2]	10
fs2	15	99	FSW2	- solar flux at the top of atm	[W/m^2]	11
fl1	15	99	FLW1	- surface downward LWR	[W/m^2]	12
fl2	15	99	FLW2	- surface upward LWR	[W/m^2]	13
fl3	15	99	FLW3	- outgoing LWR	[W/m^2]	14
rbtp	15	99	RBTP	- top atm radiation balance	[W/m^2]	15
rbsr	15	99	RBSR	- surface radiation balance	[W/m^2]	16
swa	15	99	SWABS	- absorbed in atm SW radiation	[W/m^2]	17
rwa	15	99	RWABS	- absorbed in atm LW radiation	[W/m^2]	18
ap	15	99	ALBPLN	- planetary albedo	[.]	19
q	15	99	QM	- specific humidity	[kg/kg]	20
rq	15	99	RQM	- realtive humidity	[.]	21
qi	15	99	QI	- atmospheric water content	[kg/m^2]	22
prc	15	99	PRC	- precipitation	[mm/day]	23
clds	15	99	CLDS	- stratus cloudiness	[.]	24
cldc	15	99	CLDC	- cumulus cloudiness	[.]	25
cld	15	99	CLD	- total cloudiness	[.]	26
wc1	15	99	WCLD1	- advective vertical velocity	[m/s]	27
wc2	15	99	WCLD2	- sinoptyc vertical velocity	[m/s]	28
wc3	15	99	WCLD3	- orographic vertical velocity	[m/s]	29
fh	15	99	FH	- sensible heat flux	[m/s]	30
e	15	99	EVP	- sectoral evaporation (averaged)	[m/s]	31
el	15	99	EVPL	- evaporation from land	[m/s]	32
eo	15	99	EVPO	- evaporation from ocean	[m/s]	33
qs	15	99	QS	- oceanic surface net heat flux	[W/m^2]	34
run	15	99	RUN	- total run-off	[mm/day]	35
etr1	15	99	EPOTM(1)	- pot trans from trees	[mm/day]	36
etr2	15	99	EPOTM(2)	- pot trans from grass	[mm/day]	36
prcsnw	15	99	PRCSNW	- snow fall	[m(w)/s]	38
snmlt	15	99	SNMLT	- snow melting rate	[m(w)/s]	39
as	15	99	ALBSUR	- surface albedo	[.]	40
rsms	15	99	RSMS	- relative soil moisture (150 mm)	[.]	41
fs	15	99	FRSNW	- fraction of snow	[.]	42
hs	15	99	HSNW	- snow depth	[m]	43
ft	15	99	ST	- trees fraction	[.]	44
fg	15	99	SG	- grass fraction	[.]	45
sst	15	99	SST	- sea surface temperature	[C]	46
fice	15	99	FRICE	- sea ice fraction	[.]	47
frlnd	15	99	FRGLC	- land ice fraction	[.]	48
frglc	15	99	FRGLC	- land ice fraction	[.]	48
horo	15	99	HORO	- orography	[m]	50
u	15	99	UAS	- zonal component surf wind	[m/s]	51
v	15	99	VAS	- meridional comp surf wind	[m/s]	52
acbar	15	99	ACBAR	- cross-isobar angle surf wind	[rad]	53

slp	15	99	SLP - sea level pressure	[Pa]	54
usur	15	99	USUR - module of surface wind	[m/s]	55
cd	15	99	CD - drag coefficient	[.]	56
tau	15	99	TAUXT - zonal wind stress	[N/m**2]	57
tcold	15	99	effective relative humidity		58
gdd5	15	99	convergency of diffusive flux		59
xxx	15	99	effective relative humidity		60

The yellow marked climate variables are used in this research.

Appendix II

Precession

	run O	correl	run OG	correl	run OI	correl	run OIG	correl
DJF SAT 15°S	-500	0,99	-800	0,99	-900	0,99	-1200	0,99
DJF SAT 45°S	-4900	0,99	-5300	0,97	-5000	0,99	-5200	0,98
DJF SAT 85°S	-200	0,99	-700	0,99	-700	0,99	-1100	0,99
DJF SST 15°S	-4500	0,99	-4900	0,99	-4800	0,99	-4900	0,99
DJF SST 45°S	-6900	0,99	-6800	0,98	-6400	0,99	-6300	0,98

Table 8: Table of the leads and lags in years of the filtered climate variables at the precession band (averaged over December-January-February). Columns 2, 4, 6 and 8: leads (negative, in years) and lags (positive) of the climate variables and forcings in comparison with the filtered precession signal together with the correlation(r) for run O, run OG, run OI and run OIG.

	run O	correl	run OG	correl	run OI	correl	run OIG	correl
JJA SAT 15°S	-1000	-0,99	-500	-0,99	-400	-0,99	-200	-0,99
JJA SAT 45°S	-1200	-0,99	0	-0,96	0	-0,99	+1200	-0,94
JJA SAT 85°S	-1800	-0,99	-500	-0,92	-300	-0,98	+1700	-0,86
JJA SST 15°S	-3900	-0,99	-3400	-0,98	-3400	-0,99	-2800	-0,96
JJA SST 45°S	-1100	-0,99	+400	-0,93	+900	-0,98	+2300	-0,91

Table 9: Table of the leads and lags in years of the filtered climate variables at the precession band (averaged over June-July-August). Columns 2, 4, 6 and 8: leads (negative, in years) and lags (positive) of the climate variables and forcings in comparison with the filtered precession signal together with the correlation(r) for run O, run OG, run OI and run OIG.

Obliquity

	run O	correl	run OG	correl	run OI	correl	run OIG	correl
DJF SAT 15°S	-	-	-	-	-	-	-	-
DJF SAT 45°S	+300	0,95	+3000	0,94	+4000	0,96	+4900	0,95
DJF SAT 85°S	0	0,94	+1000	0,94	+1200	0,95	+1900	0,95
DJF SST 15°S	-	-	-	-	-	-	-	-
DJF SST 45°S	+300	0,95	+2900	0,94	+4000	0,95	+4900	0,95

Table 10: Table of the leads and lags in years of the of the filtered climate variables at the obliquity band (averaged over December-January-February). Columns 2, 4, 6 and 8: leads (negative, in years) and lags (positive) of the climate variables and forcings in comparison with the filtered obliquity signal together with the correlation (r) for run O, run OG, run OI and run OIG. The results for 15S were inconclusive and therefore not taken into account.

	run O	correl	run OG	correl	run OI	correl	run OIG	correl
JJA SAT 15°S	-	-	-	-	-	-	-	-
JJA SAT 45°S	+500	0,95	+4400	0,94	+6000	0,95	+6200	0,95
JJA SAT 85°S	+400	0,95	+3500	0,94	+5000	0,95	+5600	0,95
JJA SST 15°S	-	-	-	-	-	-	-	-
JJA SST 45°S	+400	0.95	+3800	0,94	+5200	0,95	+5700	0,95

Table 11: Table of the leads and lags in years of the of the filtered climate variables at the obliquity band (averaged over June-July-August). Columns 2, 4, 6 and 8: leads (negative, in years) and lags (positive) of the climate variables and forcings in comparison with the filtered obliquity signal together with the correlation (r) for run O, run OG, run OI and run OIG. The results for 15S were inconclusive and therefore not taken into account.

95 kyr

	run OG	correl	run OI	correl	run OIG g	correl	run OIG i	correl
DJF SAT 15°S	+300	1	-1700	-1	+1000	1	-2500	-1
DJF SAT 45°S	+600	0,99	-1700	-1	+1100	1	-2400	-1
DJF SAT 85°S	+200	0,99	-1900	-1	+1000	0,99	-2500	-1
DJF SST 15°S	+700	0,99	-1500	-0,99	+1100	0,99	-2300	-0,99
DJF SST 45°S	+700	0,99	-1600	-0,99	+1200	0,99	-2300	-0,99

Table 12: Table of the leads and lags in years of the of the filtered climate variables at the 95 kyr band (averaged over December-January-February). Run OG and OIG are compared to the 95 kyr signal of the GHG-concentrations (column 2 and 6) and OI and OIG compared to the 95 kyr signal of the NH ice sheets (column 4 and 8) with the correlations (r) (column 3, 5, 7, 9).

	run OG	correl	run OI	correl	run OIG g	correl	run OIG i	correl
JJA SAT 15°S	+600	0,99	-1200	-0,99	+1200	0,99	-2300	-0,99
JJA SAT 45°S	+600	1	-1900	-0,99	+1100	0,99	-2400	-0,99
JJA SAT 85°S	+800	0,99	-1400	-1	+1400	1	-2100	-1
JJA SST 15°S	+400	0,99	-2000	-0,99	+900	0,99	-2600	-0,99
JJA SST 45°S	+900	0,99	-1900	-0,99	+1100	0,99	-2400	-0,99

Table 13: Table of the leads and lags in years of the of the filtered climate variables at the 95 kyr band (averaged over June-July-August). Run OG and OIG are compared to the 95 kyr signal of the GHG-concentrations (column 2 and 6) and OI and OIG compared to the 95 kyr signal of the NH ice sheets (column 4 and 8) with the correlations (r) (column 3, 5, 7, 9).